Master's thesis

NTNU
Norwegian University of Science and Technology
Faculty of Engineering
Department of Geoscience and Petroleum

Henrik Aas

Numerical modeling of direct shear tests of rock joints

Master's thesis in Geotechnology
Supervisor: Alexandre Lavrov
July 2023

NTNU
Norwegian University of
Science and Technology

Henrik Aas

Numerical modeling of direct shear tests of rock joints

Master's thesis in Geotechnology
Supervisor: Alexandre Lavrov
July 2023

Norwegian University of Science and Technology
Faculty of Engineering
Department of Geoscience and Petroleum

NTNU
Norwegian University of
Science and Technology

Preface

This Master's thesis marks the end of my 5-year degree and represents one full semester of dedicated work. The research presented has been undertaken during my studies at NTNU, pursuing a degree in engineering geology at the Institution of Geoscience and Petroleum. This thesis would not have been possible without the invaluable support and guidance of various individuals whom I wish to acknowledge:

First and foremost, I wish to express my gratitude to my supervisor, Alexandre Lavrov, whose mentorship has been critical in making it possible to shape and complete this work. I also want to want to thank my classmates who have supported and encouraged me to get through some academically demanding years and made the journey more enjoyable. Lastly, I want to thank my family and close friends for their support and care.

This thesis aims to contribute to the existing knowledge in the field of engineering geology. I hope it serves as a stepping stone for future researchers to build upon.

Trondheim - July, 2023

Henrik Aas

Abstract

Numerical modeling plays an increasingly larger role within fields of engineering geology. For its use in research on specific aspects of rock behavior, joint deformations under normal and shear stress have been particularly debated due to their complicated nature.

Because of this, simplified descriptions of joint deformation are often used in practical settings, which include using constant values for normal- and shear stiffness. In the context of this, direct shear tests are a common way to test the shear behavior of a rock joint. As the results of these shear tests are dependent on a large number of variables, the potential to replicate these lab tests through numerical modeling is of high interest. Though a handful of researchers have attempted this with promising results, these usually depend on advanced modeling software, which requires extensive calibration for each model. Developing functioning shear test models using more intuitive and user-friendly software makes it more convenient for researchers within the field of engineering geology to build upon the achieved results.

The work done in this thesis presents some of the rock mechanical research done over the years to highlight the challenges concerning this theoretical approach to this subject, followed by some of the research done in replicating direct shear tests numerically. Finally, work in developing a direct shear model based on saw-tooth joints under normal load/displacement created using the FEM software ABAQUS is explained in detail.

Sammendrag

Numerisk modellering spiller en stadig større rolle i felt innenfor ingeniørgeologi. For modelleringens bruk i forskning knyttet til konkrete aspekter for bergmekanikk, er sprekkdeformasjon når utsatt for normal- og skjærspenninger vært spesielt debattert grunnet deres kompliserte sammensetninger.

På grunn av dette har det vært vanlig å benytte forenklede beskrivelser av sprekkdeformasjon for praktiske formål, inkludert bruk av konstante verdier for normal- og skjærstivhet. I lys av dette har direkte skjærtester vært en vanlig måte å undersøke skjærdeformasjon av sprekker . Siden resultatene av skjærtester kan være avhengig av svært mange variabler, er muligheten for å replisere disse testene numerisk av høy interesse. Selv om enkelte forskere har forsøkt å gjøre dette og oppnådd lovende resultater, er disse modellene ofte avhengig av omfattende kalibrering for hver enkelt modell. Med utvikling av modeller for skjærtester gjennom intuitive og brukervennlige programvare, vil det være enklere for andre ingeniørgeologer med begrenser erfaring innen modellering å bygge videre på de oppnådde resultatene.

Arbeidet gjort i denne masteroppgaven presenterer noe av den bergmekaniske forskningen gjort over årene for å belyse utfordringene knyttet til de teoretiske tilnærmingene til dette tema. Videre, undersøkes noen andre forsøk gjort på å gjenskape skjærtester numerisk. Til slutt presenteres arbeidet gjort i utvikling av direkte skjærtester basert på "Saw-tooth"- sprekker under normallast/deformasjon, laget gjennom det FEM-baserte modelleringsprogrammet ABAQUS.

Contents

1 Introduction **1**

2 Theory **3**
2.1 Shear strength of rock joints . . . 3
2.2 Joint deformation and joint stiffness . . . 5
2.3 JRC and Saw-tooth asperities . . . 7
2.4 Methods for measuring shear stiffness and mathematical descriptions . . . 8
2.5 Scaling effect in rock joints . . . 12
2.6 Experimental studies of joint shear stiffness using saw-tooth models . . . 14
2.7 Numerical studies in literature . . . 17
2.8 Modeling in ABAQUS . . . 20

3 Model development for numerical shear tests **22**
3.1 Sensitivity study of normal stress models . . . 24
3.2 Numerical setup . . . 24
3.2.1 Mesh . . . 25
3.2.2 Interaction . . . 26
3.2.3 Post-processing . . . 27
3.3 Normal closure with different surface geometries . . . 28
3.3.1 Flat surface joint . . . 28
3.3.2 Matched saw-tooth joint . . . 29
3.3.3 Hand-drawn joint surface: . . . 30
3.4 Shear without normal load . . . 31
3.4.1 Boundary Conditions for elastic 2D models . . . 33
3.4.2 CNL and CND conditions . . . 34
3.4.3 Sensitivity studies - results . . . 34
3.5 Elastic CND model - Shear under normal displacement . . . 35
3.5.1 Elastic CND with scaled joint surface . . . 39
3.5.2 Elastic CND at different Young's modulus . . . 40
3.5.3 Elastic CND at different Poisson's ratio . . . 41
3.5.4 Elastic CND with different mesh geometry . . . 41
3.6 Elastic CNL models - shear under normal load . . . 43
3.6.1 Use of time period in CNL . . . 45
3.7 Plastic 2D CNL model . . . 49
3.8 35.degree plastic CND model . . . 52

4 Discussion **54**
4.1 Evaluation of model aspects . . . 54
4.1.1 Parts . . . 54
4.1.2 Mesh . . . 54
4.1.3 Interaction properties . . . 55
4.1.4 Material Parameters . . . 55
4.1.5 Boundary conditions . . . 55

4.1.6 Post-processing 56
4.2 Evaluation of simulated joint behavior 56

5 Conclusion **60**

List of Figures

2.1 Mohr coulomb (1) and Patton (2) shear stress (N.R Barton 2013) 3
2.2 Regression study between tangential Young's modulus and uni-axial compression strength (UCS) 4
2.3 Joint deformation/stress curves for normal stress applied to a solid sample, interlocked joints, and mismatched joints (S.C Bandis et al. 1983) 6
2.4 Typical results from shear tests under CNL conditions (Barton and Choubey 1977) 8
2.5 Shear stiffness measured using secant and tangent method (Packulak et al. 2022) 9
2.6 JRC profiles Barton and Choubey 1977 10
2.7 Shear strengths-normal strength of saw-tooth triangular joints from Patton, Firhurst and Ladayni models (Bahaaddini et al. 2013) 11
2.8 JRC effect on strength deformation trends Barton and Bandis 1982 (left). Numerical simulations by Bahaaddini et al. 2013 shows the same trend (right) 12
2.9 Examples of dealing with scaling based on JRC 14
2.10 Shear stress displacement curves for regular saw-tooth joints of $15° - 15°$ (left), $30° - 30°$ (right) at different initial normal pressure for CNL and CNS conditions (Shrivastava et al. 2015) 15
2.11 Lab results effect of initial normal load for shear strength (Shrivastava et al. 2015) 15
2.12 Indication of fracturing during shear simulations at various normal loads and dilation angle of saw-tooth triangular asperities 17
2.13 Numerical joint closure. (a) Top view of lattice-grid cylindrical asperities. (b) Side view of initial asperities before normal load. (c) asperities after applied normal load (L. Wang et al. 2016) 19
2.14 Numerical joint closure. (a) Top view of lattice-grid cylindrical asperities. (b) Side view of initial asperities before normal load. (c) asperities after applied normal load (L. Wang et al. 2016) 20
3.1 Initial setup for CNL and CND first load step 24
3.2 Quad mesh with seeding set to 1 26
3.3 Interaction with master- and slave surface 27
3.4 Path along the bottom part of the bottom block with all adjacent elements included used for exporting reaction forces 28
3.5 Model setup and stress distribution for elastic flat surface model 28
3.6 Stress-strain output for flat surface elastic model 29
3.7 Model setup for elastic 15 deg saw-tooth model 29
3.8 Stress-displacement of mismatched hand-drawn asperities under constant normal displacement 30
3.9 Stress magnitude of last converged increment of normal displacement . . 30
3.10 Stress-displacement of mismatched hand-drawn asperities under linear normal displacement 31

3.11 Stress-strain plot for elastic shear of 15 deg. Saw-tooth asperities until last converged increment . . . 32
3.12 Stress magnitude at last converged increment of CND Elastic shear model 32
3.13 Shear displacement at last converged increment of CND Elastic shear model 33
3.14 Boundary conditions for flat surface model . . . 34
3.15 Setup for elastic CND 2-step normal and shear displacement . . . 36
3.16 Boundary condition setup for CND model . . . 37
3.17 Shear-displacement plot elastic CND for normal displacement (0.01mm, 0.02mm, 0.03mm, and 0.05mm) . . . 37
3.18 Summary of results from elastic CND models . . . 38
3.19 BC setup for 15.degree CND model with joint length scaled up to 200mm 39
3.20 Stress-displacement plot for Elastic CND model with scaled joint length . 39
3.21 Shear stress-displacement for CND model using different Young's modulus 40
3.22 Shear stress-displacement for CND model using different Poisson's ratio . 41
3.23 Bottom part of the saw-tooth model with quad- and tri-mesh elements . 42
3.24 Shear stress-displacement for CND model using different mesh types . . . 42
3.25 Concept illustration of CNL model . . . 43
3.26 Shear stress-displacement for CNL to last converged increment . . . 44
3.27 Vertical displacement for CNL at 1 MPa normal load. Non-uniformly distributed normal displacement . . . 45
3.28 Shear displacement when defining the time periods of the shear step as 1, 10, and 100 seconds. . . . 46
3.29 Normal displacement during shear load of frictionless CNL model . . . 46
3.30 Shear stress-displacement for CNL to last converged increment . . . 47
3.31 Normal displacement for the left and right side of the top block during a CNL shear test . . . 47
3.32 Shear stress-displacement plot for CND at 0.05mm normal displacement and CNL at 5 MPa normal pressure . . . 48
3.33 Stress (left) and AC Yield (right) of plastic CNL simulation . . . 50
3.34 Stress-displacement plot of 15.degree CNL model with and without added plastic parameters (M-C) . . . 51
3.35 Stress (left) and AC Yield (right) of plastic CND simulation . . . 51
3.36 BC setup for 35.degree asperity plastic model . . . 52
3.37 Stress result and yielded elements for 35.degree asperity plastic model . . 53
3.38 Stress-displacement plot for 35.degree asperity plastic model . . . 53
4.1 Linear stiffness (tangent and secant) for elastic CND model . . . 58

List of Tables

3.1 SI and SI(mm) unit system . . . 22
3.2 Properties for the first test models . . . 25
3.3 Normal load and displacement for 15-degree elastic saw-tooth model . . . 36
3.4 Results of CND at different initial normal displacement . . . 38

3.5 Shear-displacement results at different Young's Modulus (E) 40
3.6 Shear-displacement results at different Poisson's ratio (ν) 41
3.7 Shear-displacement results with different mesh types 42
3.8 Elastic CNL results 44
3.9 Input for Plastic 2D CNL model 50
4.1 Linear secant shear stiffness measured for elastic CND models with 15.degree triangular asperities at different normal displacement 57
4.2 Linear secant shear stiffness measured for elastic CND models with 15.degree triangular asperities at different normal displacement 58
4.3 stiffness results for elastic CND models at different normal displacement (Figure 3.18) 58
4.4 Shear stiffness for some of the models using different stiffness criteria (all values in [MPa/mm]) 59

1 Introduction

Understanding the deformation characteristics of rock masses is essential in engineering geology, rock mechanics, and related areas that involve structures in the rock mass, slope stability, and tunnels. In low-stress situations like land-based geomechanics, joint deformation, the deformational behavior of rock mass is mostly dominated by the joint behavior. However, the mathematical description of joint deformation has been a topic of extensive debate in literature for the past century. Accurate calculations necessitate specific parameters for each individual joint, some of which may not always be available, leading to the requirement of simplifications in certain situations. For more complex scenarios, more complex models are necessary to match these deformations. As a result, over time, numerous mathematical models and, eventually, numerical approaches have been developed.

As the primary deformation factor for rock mass relates to the closure of joints in low-stress situations, the terms normal stiffness k_n and shear stiffness k_s are used to describe deformation during joint closure when exposed to normal stress and shear stress respectively. Despite a number of different mathematical models debating the non-linear nature of this deformation process, Goodman's 1967 linear model is still commonly used, as they are fairly simplistic and don't rely on an extensive amount of input parameters. However, the studies debate whether more complex mathematical models are better suited for certain situations, as the more realistic hyperbolic deformation stage is not neglectable in many cases.

With the need for better mathematical descriptions of these closure-deformation processes, a great deal of research has been done over the past half-century to understand this behavior better. Both normal- and shear stiffness can be determined through laboratory tests on rock core samples or through in-situ testing. Normal stiffness has, for instance, been calculated through compression tests of mismatched joints. For shear stiffness, borehole shear testing or plate load testing are examples of methods that can be used. One more common method is, however, direct shear testing under normal load, using a shear box. This is an easily repeatable lab test, as it's possible to adjust the sample size and loads for test comparisons.

Despite a large amount of documented laboratory test results for the mentioned tests, the complex nature of rock mass makes it difficult to make representative empirical data for different rock types and other characteristics. The main factors determining stiffness may vary drastically so that unique combinations of these parameters will always occur.

With increasingly more powerful computer technology, numerical modeling has been used as a method of simulating the behavior of rock mass under different stress-related circumstances. Some of the parameters used to describe the mechanical properties of a rock mass (Young's modulus, Poisson's ratio, friction angle, JRC, JCS, etc.) may be used in numerically simulating rock mass in different scenarios, which is useful both in practical modeling in engineering geology. More specific cases in rock mechanics, such as the laboratory tests for normal and shear load, have been done using other software such

as ABAQUS and PFC. Direct shear test for rough joints has been modeled in discrete element software PFC2D, using parallel bond models to simulate joint fractures (Bahaaddini et al. 2013). This particular study also used a smooth joint model. Other numerical studies include Liu et al. 2020, simulating shear tests under constant normal load, constant stress, and constant displacement while comparing the differences. Though both of these studies were successful in replicating physical direct shear tests under normal load, both come with disadvantages. First off, the bond removal model requires carefully calibrated micro-parameters, which can be difficult to obtain, and thus impractical to use in many cases. The smooth joint model also showed an exaggerated increase in shear strength with increased shear load (Bahaaddini et al. 2013).

For the use of numerical modeling for the described purposes, ABAQUS has the advantage of using familiar mechanical parameters for engineering geologists in terms of fracture criteria/plasticity, interaction parameters, etc. This particular software is also relatively user-friendly, making it more convenient for students and engineers with limited experience in modeling, making it possible to achieve realistic results without the use of more advanced modeling software that requires a good amount of experience with modeling.

In the context of the shear behavior of rock joins, one method that has been used in both numerical and experimental studies is a shear test with surfaces with symmetrical, triangular joint asperities (saw-tooth joints). With these saw-tooth models, roughness is represented by the angle of the triangular asperities, equivalent to the dilation angle for a joint roughness coefficient (JRC). This way, it is possible to eliminate some of the uncertainties that come with comparing JRC surfaces, as they are difficult to replicate for comparison between numerical and experimental studies. When studying shear behavior in ABAQUS, surface generation can also be done without the use of external software as they are simple to recreate with the sketching tools in the ABAQUS software.

This thesis contains a detailed walkthrough of the development of a numerically simulated direct shear test under both constant normal load and constant normal displacement. Different aspects of the setup and results of this development work have been based on relevant theory and similar numerical work and evaluated.

2 Theory

2.1 Shear strength of rock joints

For a general description of rock mass behavior under stress, a number of mathematical models are commonly used. Some of the most used include Mohr-coulomb (equation 2.1). Patton expanded on this with another, steeper, linear step from 0, adding the dilation angle to the friction angle, resulting in a bi-linear model (Figure 2.1). The first step here can be described by equation 2.2, with the second part being the Mohr-Coulomb criterion.

$$\tau = \sigma_n tan\phi_r + c \tag{2.1}$$

with τ being the shear stress, σ_n being normal stress, ϕ_r residual frictional angle, and c being cohesion.

Patton adds to the Mohr-Coulomb with a cohesion step having a steeper linear normal-shear relation at first due to surface roughness.

$$\tau = \sigma_n tan(\phi_r + i) \tag{2.2}$$

Where the added parameter i is the dilation angle.

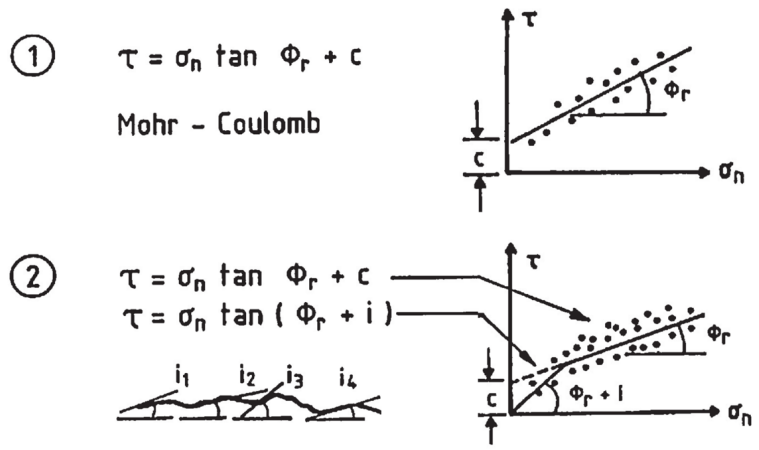

Figure 2.1: Mohr coulomb (1) and Patton (2) shear stress (N.R Barton 2013)

In the context of the numerical study of rock behavior, some conflicts occur when comparing literature where certain mechanical aspects are lacking. For instance, parameters such as JRC and JCS are needed in the stiffness formula (equation 2.9). In order to have the possibility of using this equation when some necessary parameters are lacking, some estimations are used.

For elastic modeling in ABAQUS, E-modulus is a required mechanical parameter for a contact model. However, the UCS value may not be included as a material parameter,

which is inconvenient when compared to experimental data, as UCS is much more commonly included in the results of any given lab research. In cases of comparing numerical models with different inputs, an estimation based on empirical data could be sufficient. Figure 2.2 shows the result of an empirical study between UCS, Young's modulus, and Schmidt Hammer data (Sachpazis 1990). Results found the linear empirical relation to be the following (equation 2.3) (figure 2.2):

$$E\,[GPa] = 0.3752 \cdot UCS\,[MPa] + 4.428 \tag{2.3}$$

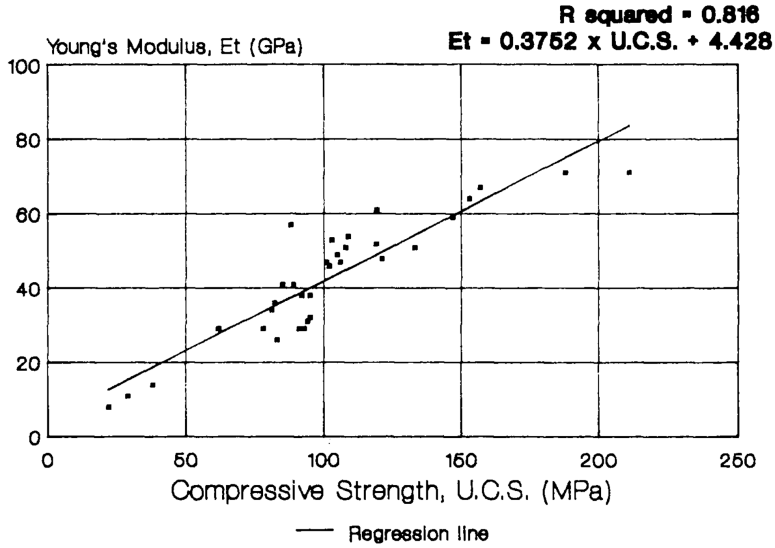

Figure 2.2: Regression study between tangential Young's modulus and uni-axial compression strength (UCS)

As this estimation is the empirical result of tests from a vast selection of rock types, it comes with a large standard deviation and is, for that reason, too unreliable in most cases. For the sake of using estimated JCS as a placeholder for actual measured data, it may serve the purpose of comparing results from numerical simulations.

For the purpose of estimating UCS values for a given E-modulus lower than 4.428 GPa, another estimation must be used as equation 2.3 will result in a negative value. Y. Wang et al. 2016 includes a number of other simplified correlations for this purpose. The research included a linear regression estimate for sandstone, which concluded equation 2.4 to be a viable estimate (Malik et al. 1997).

$$UCS[MPa] = 0.0084 \cdot E[MPa] \tag{2.4}$$

In theory, the dilation angle should be equal to the JRC value, given that the joint is under low normal stresses and the surface is undamaged (Barton and Choubey 1977). With increased stress, the dilation angle could be higher.

2.2 Joint deformation and joint stiffness

Joint deformability can be described by the character of the joint deformation curve (R.E Goodman et al. 1968). In that context, the terms normal stiffness and shear stiffness were introduced to describe the rate of change of stress and displacement (equations 2.5 and 2.6).

$$k_n = \frac{\sigma_n}{u_n} \tag{2.5}$$

Where σ_n and u_n are normal stress and displacement.

$$k_s = \frac{\tau}{u_s} \tag{2.6}$$

Where σ_s and u_s are shear stress and displacement.

This could be done by observing the stress and displacement, along with maximum joint closure, peak- and residual shear displacement, and maximum joint closure. The mechanics of joint normal deformation could be described by considering how maximum closure has to be less than the maximum gap anywhere along the mated walls. The experimental studies done by Goodman showed that the normal load of non-matching rock joints created a hyperbolic stress-displacement relation. Similar studies have followed up Goodman's work. Hungr et al. 1978 again defining linear relations, attributing this to "precompression effects" due to previous load history. Snow 1972 further confirmed this by addressing how hyperbolic closure is applied to joints that have not been previously closed.

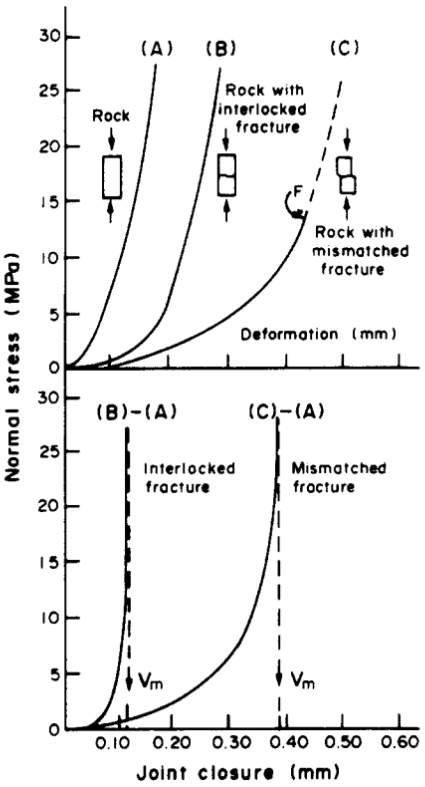

Figure 2.3: Joint deformation/stress curves for normal stress applied to a solid sample, interlocked joints, and mismatched joints (S.C Bandis et al. 1983)

As an improvement on Goodman's hyperbolic model, S.C Bandis et al. 1983 proposed a number of relationships, including stiffness criteria based on the parameters maximum joint closure V_m and initial normal stiffness k_{ni} (equation 2.7). Another proposition included a semi-logarithmic law with the implication that a joint never reaches the maximum closure. (equation 2.8)

$$k_n = k_{ni}(1 - (\frac{\sigma_n}{V_m k_{ni} + \sigma_n}) \tag{2.7}$$

$$k_n = \frac{q\sigma_n}{log_{10}e} \tag{2.8}$$

Similar to joint normal stiffness, shear stiffness describes the shear stress with respect to shear displacement. The shear stiffness is measured prior to the yield stage when inducing shear movement under a specified normal load. The linear component of the linear-elastic portion of the measurements represents the onset of shear displacement to yield shear stress.

Shear stiffness was further researched experimentally in S.C Bandis et al. 1983. When observed in the pre-peak range, it was found to have hyperbolic stress-deformation curves. Here, the expression in equation 2.9 was able to describe this relation.

$$k_s = \frac{100}{L} \cdot \sigma_n tan[JRC\, log_{10}(\frac{JCS}{\sigma_n} + \phi_r)] \tag{2.9}$$

Where JCS (joint wall compression strength) is equal to the uni-axial compression strength (σ_c) or UCS. L is the initial joint length introduced in order to address the scale effect, as the stiffness was shown to decrease with longer joints. The equation is under the assumption that the peak shear strength is reached and 1% of the joint length is sheared. Another important note is that the anisotropy of k_n/k_s levels are higher at low stress levels.

In other research, normal joint stiffness is determined by subtracting the displacement of an intact sample under normal load from the displacement of a mismatched horizontal joint of the same specimen (equation 2.10). Shear stiffness can likewise be measured using direct shear testing under different normal loads. A challenge in both these circumstances is due to the heterogeneous nature of rock specimens, as samples of even similar rock types may not be expected to give similar results (Kulatilake et al. 2016).

$$D_j = D_{rm} - D_i \tag{2.10}$$

D_j is the joint normal deformation of a rock specimen under normal stress, D_i is the deformation of the intact sample, and D_{rm} is the deformation of a normal joint. Interpreting the results of direct shear tests of natural rock pose challenges due to the repeatability of the sample (Shrivastava et al. 2015)

2.3 JRC and Saw-tooth asperities

Both numerical and experimental research of shear behavior varies in some aspects in terms of execution, surrounding sample adjustment, surface conditions, and stress conditions. In terms of stress conditions, shear tests are commonly separated into the following:

- Constant normal load (CNL): The top block is a pressure load that remains unchanged throughout the shear test
- Constant normal displacement (CND): The distance between the top part of the top shear block and the bottom part of the bottom block remains unchanged for the shear test
- Constant normal stiffness (CNS): Linear normal stiffness [MPa/mm] remains unchanged for the shear test. Stiffness criteria may vary for different studies

For FEM modeling work, CNS conditions are difficult to achieve when defining boundary conditions. Results from different direct shear tests are naturally heavily dependent on the mechanical parameters of the material. However, under the listed stress conditions, similar stress-displacement curves are typically recreated. Figure 2.4 shows typical shear test results based on shear tests of a multitude of specimens varying in origin and mechanical properties but with similar normal load and joint roughness.

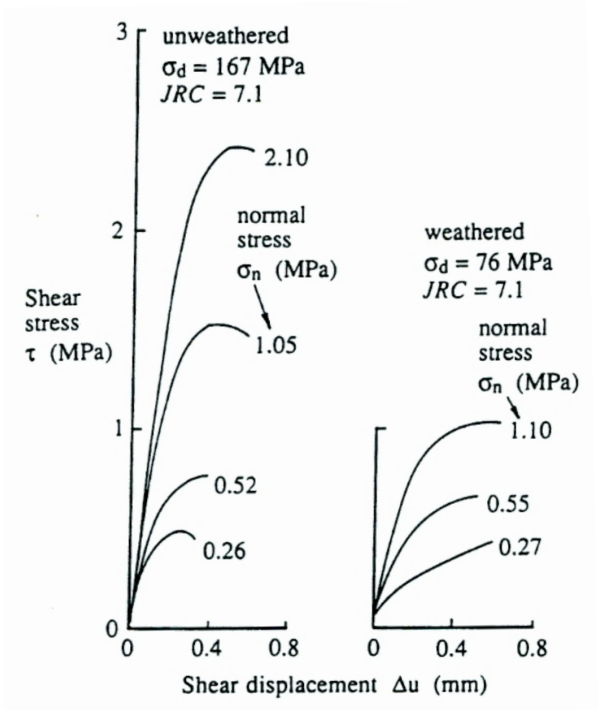

Figure 2.4: Typical results from shear tests under CNL conditions (Barton and Choubey 1977)

In a model development setting, when using experimental data found in literature as a reference, all necessary material parameters might not always be available. In such cases, achieving similar stress-displacement curves is a good reference point.

2.4 Methods for measuring shear stiffness and mathematical descriptions

Given the multiple methods in approaching shear stiffness, upon reviewing experimental studies, some occurred more than others. Among the more common ones are:

- Goodman 1970 – secant (peak) method
- Hung and Coates 1978 – tangent (yield) method
- Kulhway 1975 – Hyperbolic model
- Day 2017 – Best fit chord measurement

Among the mentioned, the Secant Peak Method (RE Goodman 1970)and the Tangent Yield Method (Hungr et al. 1978) are the most used. The secant shear stiffness can be defined as the secant between zero and peak applied shear stress when plotted versus shear displacement. Though convenient, this does not account for sample seating (matching) or asperity softening, which can lead to non-linearity of shear stress displacement (Packulak et al. 2022). The tangent stiffness method can be measured in one of two ways; As the tangent at 50% of shear stress or by approximated best fit between 40% and 60% of the peak shear stress. In a study conducted on samples of granite for both smooth surfaces

and fractures, these two measuring methods were compared. The results showed the secant shear stiffness to be much lower than the tangential shear stiffness in many cases.

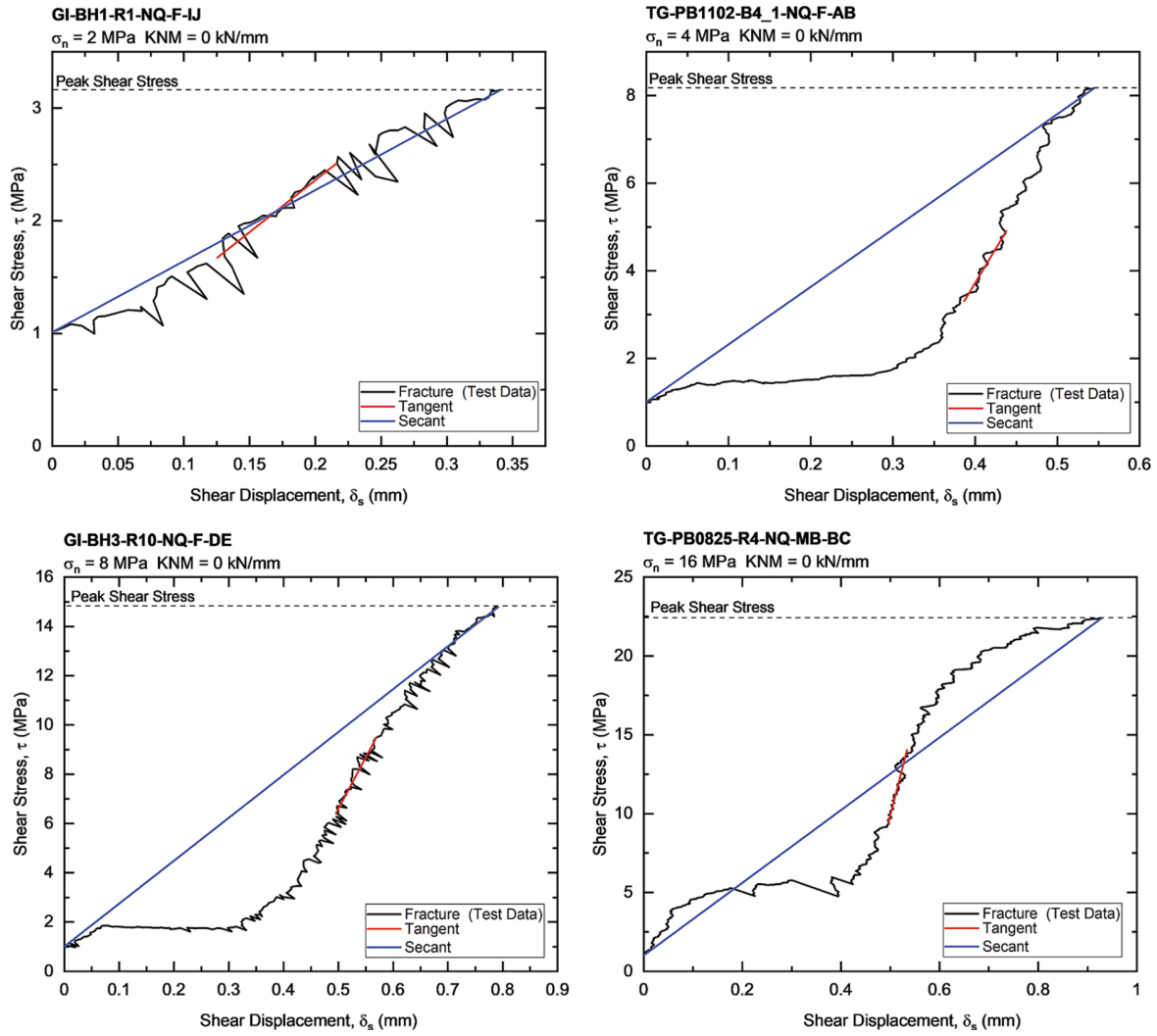

Figure 2.5: Shear stiffness measured using secant and tangent method (Packulak et al. 2022)

As shown in Figure 2.5, with irregular deformation patterns, the different stiffness output may be drastic depending on what stiffness measuring method is used. Four of these are shown with both the secant and tangent method for samples where a longer "stabilizing stage" resulted in a higher stiffness when using the tangent method. In cases where fracture apertures are close to being matched, this difference is smaller.

Figure 2.6 shows some common roughness profiles for different rock types. These profiles are commonly used in numerical studies like Bahaaddini et al. 2013 and Liu et al. 2020 as imported geometry for 2D joint surfaces. In terms of scale effect, rougher profiles may have larger, non-representative asperities, which can highly affect the results of a small-scale shear test. Obtaining JRC value is typically done by visual comparison of these profiles. In situations that require precise comparison between models, the JRC value could also be acquired using back-calculation of the equation 2.11.

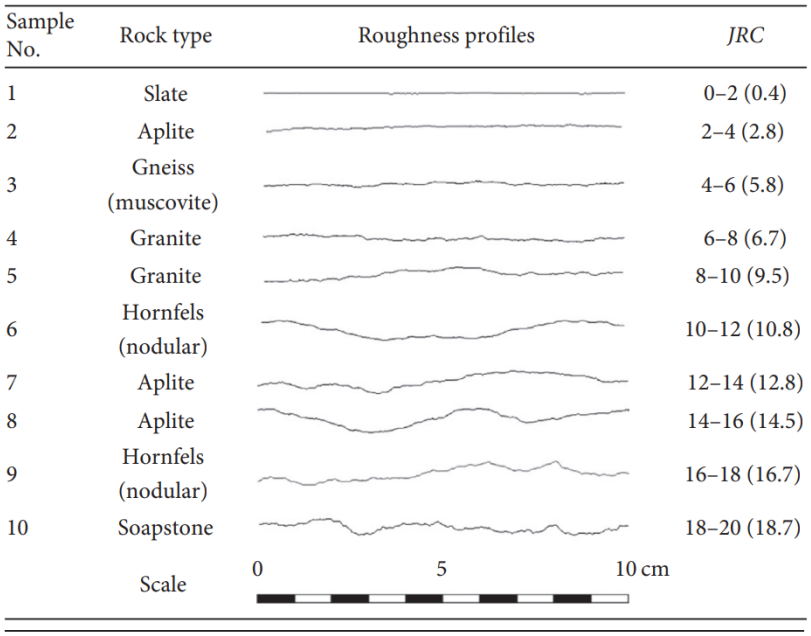

Figure 2.6: JRC profiles Barton and Choubey 1977

$$d_n = \frac{1}{M} JRC \cdot log(\frac{JCS}{\sigma_n}) \tag{2.11}$$

Where M is the damage coefficient, which again can be obtained from equation 2.12:

$$M = \frac{JRC}{12 \cdot log(JCS/\sigma_n)} + 0.70 \tag{2.12}$$

Using the Patton shear strength criteria, shear strength may also be used for saw-tooth triangular asperities (Patton 1966). This model uses transmission stress (σ_T), which is calculated through equation 2.13.

$$\sigma_T = \frac{C_j}{tan\,\phi_\mu - tan\,\phi_r} \tag{2.13}$$

With C_j being cohesion of asperities, and ϕ_μ and ϕ_r being friction angle and residual friction angle.

In that case, the shear strength can be described by equation 2.14 and 2.15

$$\tau = \sigma_n tan(\phi_\mu + i) \quad for \quad \sigma_n < \sigma_T \tag{2.14}$$

$$\tau = c_j + \sigma_n tan\,\phi_r \quad for\ \sigma_n > \sigma_T \tag{2.15}$$

Although this model is fairly simplistic while lacking aspects of parameters such as joint cohesion and complexity in surface geometry, it does provide useful insight into shear behavior.

Another model, based on energy principles, may also be used to describe sliding and shearing mechanisms (Ladanyi et al. 1969)

$$\tau = \frac{\sigma_n(1 - a_s)(\dot{\nu} + tan\,\phi_\mu) + a_s\,S_R}{1 - (1 - a_s)\dot{\nu}\,tan\,\phi_\mu} \tag{2.16}$$

Adding parameters a_s as shear area ratio, $\dot{niu}$ as dilation rate, and S_R as intact rock strength. Rock strength can be obtained from the Fairhurst intact strength criterion (Fairhurst 1964). Here, n is the ratio of tensile to uni-axial compression strength:

$$S_R = \sigma_c \frac{\sqrt{n+1} - 1}{n}[1 + n \cdot \frac{\sigma_n}{\sigma_c}]^{0.5} \tag{2.17}$$

In Ladanyi et al. 1969 experimental study was used extensively to express empirical power laws from saw-tooth triangular joints.

The results concluded the constants k_1 and k_2 as 1.5 and 4.0 respectively. Shortcomings in using this model included difficulty in obtaining the σ_T constant, as well as the dilation for irregular joints.

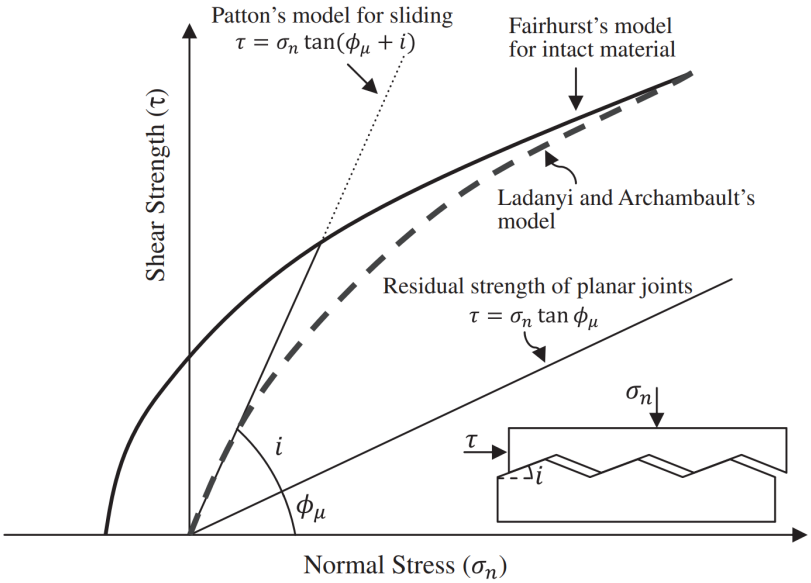

Figure 2.7: Shear strengths-normal strength of saw-tooth triangular joints from Patton, Firhurst and Ladayni models (Bahaaddini et al. 2013)

Based on experimental data from Shrivastava et al. 2015, the $30° - 30°$ asperity typically creates the stress-displacement pattern shown in Figure 2.8 under constant normal load (CNL) conditions with relatively low normal stress.

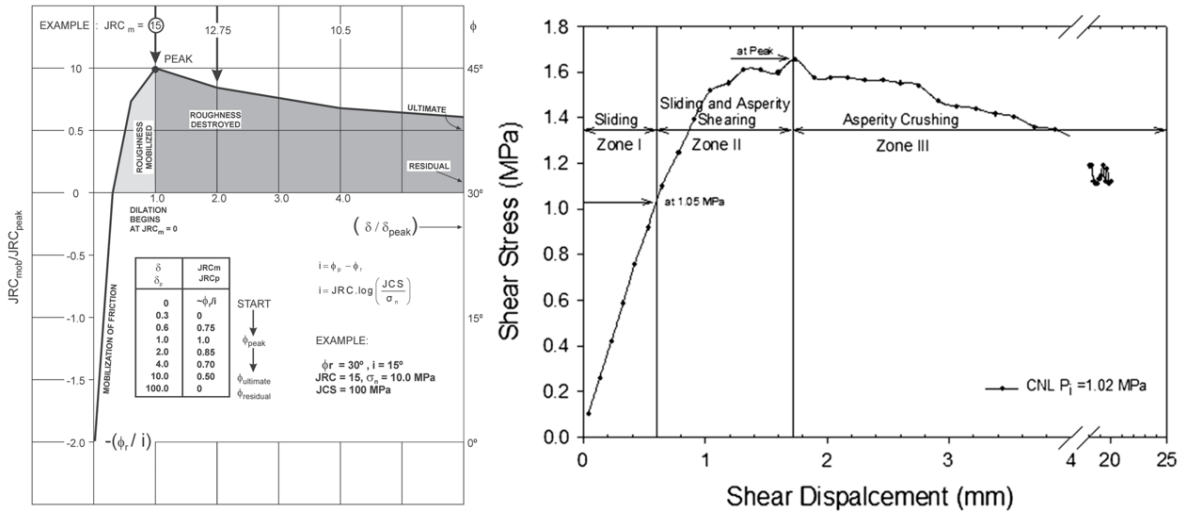

Figure 2.8: JRC effect on strength deformation trends Barton and Bandis 1982 (left). Numerical simulations by Bahaaddini et al. 2013 shows the same trend (right)

The shear stress-displacement relation with shearing under normal load can typically be described as shown on the right side of Figure 2.8. This deformation will, in many cases, contain a nonlinear phase at the beginning due to softening of the asperities in the linear phase where stiff/elastic deformation occurs. Before peak shear strength is reached, there is a gradual softening, which in the case of this example, is between 1.3 MPa to 1.6 MPa. For the right side, these were the simulation results for the shearing behavior of a $30° - 30°$ saw-tooth triangular asperity shear stress-displacement behavior under CNL conditions.

2.5 Scaling effect in rock joints

As explained by Barton, the scaling effect of shear behavior creates challenges in rock engineering scenarios. Several studies have been done in order to quantify and establish empirical relations at different scales of shear movement, also addressing the other contributing factors in this aspect. The proposed relation from Barton and Choubey can be explained by equations 2.18, 2.19, and 2.20, with L_n and L_0 being respectively in-situ and normal size of the specimen (normally at 100mm).

$$\tau_{peak} = \sigma_n tan[JRC \cdot log(\frac{JCS}{\sigma_n}) + \phi_b] \tag{2.18}$$

$$JRC_n = JRC_0[\frac{L_n}{L_0}]^{-0.02JRC_0} \tag{2.19}$$

$$JCS_n = JCS_0[\frac{L_n}{L_0}]^{-0.02JRC_0} \tag{2.20}$$

Essentially this suggests that the max shear stress decreases with increasing joint size. This can also be referred to as the "negative scale effect".

Other studies observe a positive scale effect when τ_{peak} increases (Locher et al. 1970). Meanwhile, some studies have not found any obvious scale effect (Hencher et al. 2020). The inherent difficulty in obtaining and carrying rock samples on a sufficient scale is one of the main reasons for the limited research.

One shear test method by Ueng et al. 2010 was based on reducing, enlarging, and re-assembling a single joint profile up to 300 mm joint length. In this study, no scale effect where apparent. However, similar to other large-scale experiments, this study was not conducted under CNS conditions but rather closer to CNL, which was not considered in small-scale studies like Shrivastava et al. 2015 and numerical simulations in Liu et al. 2020. As a consequence, the correlation between the results obtained from different scales is uncertain.

Shear stiffness under CNS conditions can be expressed as shown in equation 2.21 as a general expression of the normal pressure conditions during shear tests.

$$\sigma_n(t + \delta t) = \sigma_n(t) + k_n \delta d \tag{2.21}$$

With t being the time increment, d being displacement, k_n normal stiffness, and σ_n normal stress.

In addition to the difficulties surrounding the k_n parameter, as discussed in earlier sections er, we can also see from the equation that for a high k_n, the normal displacement is extremely small and may be ignored. In regards to shear tests under constant normal displacement, where the normal displacement is fixed at zero during the shear displacement. In this case, the normal stiffness will be infinite, as shown in equation (2.21).

Generally, CNS and CNL conditions are most relevant for shallow rock joints where normal deformation resulting from the shear movement of a joint is, to a larger extent, allowed to occur. For modeling purposes, this creates another challenge as FEM models can only induce one of either displacement or stress while calculating the other (ABAQUS-Manual 2014).

A common approach in dealing with the scaling effect is to use small joint specimens that are cut from larger ones (Giani et al. 1995). Another one is to use partial replicas of larger joints (Castelli et al. 2001). A third approach used by Lou and Ueng (Ueng et al. 2010) is by enlarging the established JRC profiles or assembling them in order to generate larger joints: In Lou, 100mm, 200mm, 400 mm, and 800mm were simulated in this way using standard JRC-profiles. All of the samples were 100mm in height.

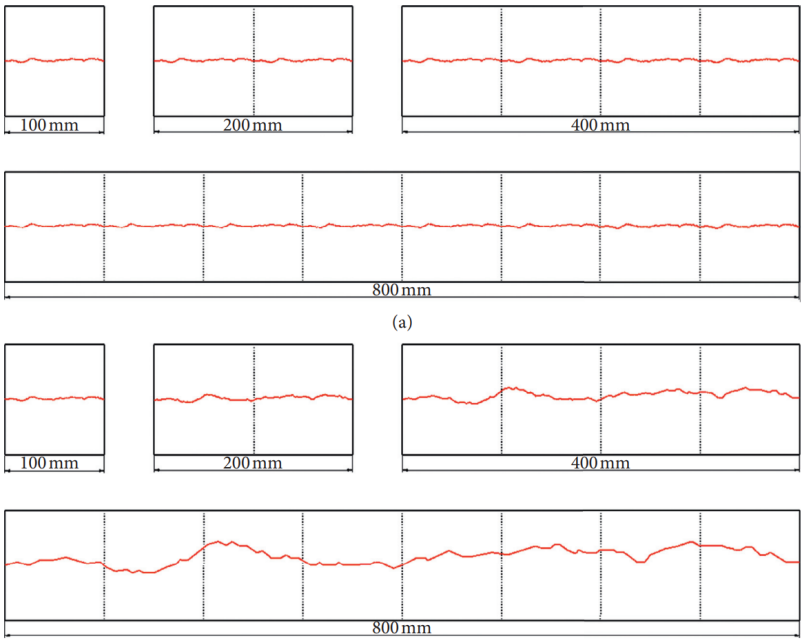

Figure 2.9: Examples of dealing with scaling based on JRC

Figure 2.9 demonstrated different ways of approaching scaling for JRC profiles. In (a) the 18-20 JRC roughness profile from Figure2.6, the profile is copied and connected in a series to the desired joint length. In (b), the joint is generated for the desired length of the total sample so the original JRC profiles cover the total length.

2.6 Experimental studies of joint shear stiffness using saw-tooth models

For the physical study of shear tests on saw-tooth joints, one study was found and evaluated. Shear stiffness was studied on samples with saw-tooth triangular joint asperities, varying from 90 - 15 degrees. The same study included tests on irregular joints using rough surfaces with JRC values determined based on visual inspection (Shrivastava et al. 2015).

Using a direct shear apparatus consisting of a loading unit, a hydraulic power pack, and a control unit, joint samples were able to be tested in both CNL and CNS boundary conditions. All samples tested were approximately 300 mm $\times$ 300 mm $\times$ 448 mm. In order to avoid frictional forces between the sample, a 5mm needle linear bearing was placed between the mated walls. The material used to stimulate soft rock was a mix of Plaster of Paris (POP), commonly used as a reproducible testing material with predictable characteristics. As the experimental studies were not tested on rock samples, factors relating to the non-homogeneous nature of rock mass are not factored in this study.

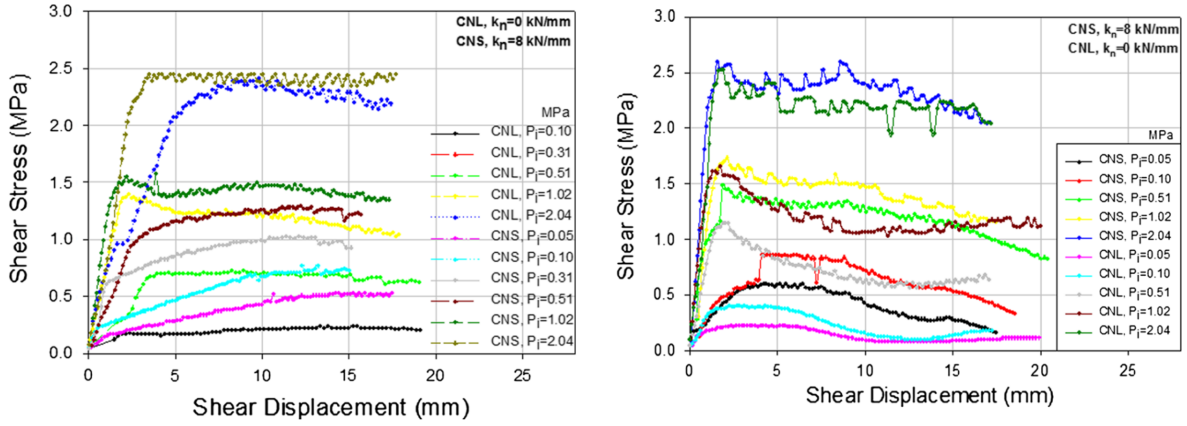

Figure 2.10: Shear stress displacement curves for regular saw-tooth joints of $15° - 15°$ (left), $30° - 30°$ (right) at different initial normal pressure for CNL and CNS conditions (Shrivastava et al. 2015)

Figure 2.10 show the test results from Shrivastava et al. 2015 direct shear tests. For the CNL test, normal stiffness was set to $k_n = 0kN/mm$ while at CNS $k_n = 8kN/mm$. The stress-displacement behavior is here characterized by the peak, which in this case is well defined. By viewing the plots, it's clear that the CNL cases under-predict the shear strength compared to CNS conditions. At the point where the curve flattens out, the stress is constant, which is most clear at the highest P_i in CNS.

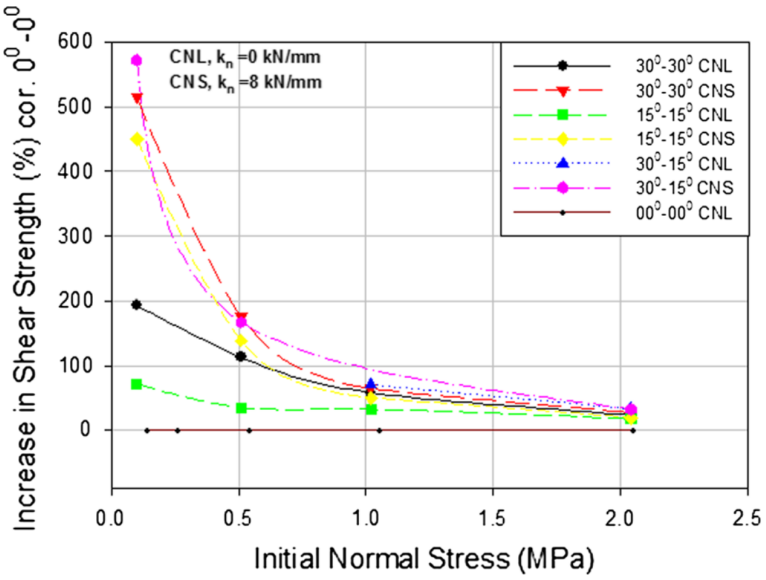

Figure 2.11: Lab results effect of initial normal load for shear strength (Shrivastava et al. 2015)

From observing the shear tests at different levels of initial normal stress P_i and dilation angles, results show that the increase of asperity angles increased the shear strength. This had a larger effect under CNS than CNL conditions due to the degradation of asperities being higher. Likewise, the frictional resistance is higher under CNS conditions which

contributes to the same effect. However, with increasing P_i, this effect was reduced. With P_i being higher than 18% of UCS, the shear strength under CNL and CNS conditions were approximately the same (Figure 2.11). In the range between 9% UCS and 18% UCS, the curvature of the shear strength increase with increased dilation angle for both CNL and CNS. When using irregular geometry of the joint surface, the results showed a higher shear strength than the regular profiles. Regular joints had a linear strength envelope. In both CNL and CNS, the strength envelope changed to curvilinear for non-planar joints. The model created was successful in predicting shear strength for rock types ranging in hardness.

While CNS conditions lead to a strain-softening behavior, CNL leads to strain-hardening. For CNS, this can be seen from how the normal stress increase with shear displacement before the shear displacement reaches the length to the top of the asperity at 8.66mm for the 30° roughness; after that, the normal load decreases until it reaches a minimum value, which again is equal to initial normal load (Shrivastava et al. 2015). These principles are not applicable if using JRC as the roughness parameter.

The shear strength model proposed is based on the experimental research by Shrivastava et al. 2015 on Patton's bi-linear strength model. This is only valid when dilation is not restricted, and the joint is only subjected to low normal stress.

2.7 Numerical studies in literature

The numerical modeling work by Bahaaddini et al. 2013 follows a typical direct shear test setup, similar to Shrivastava et al. 2015, with a 100mm block in length and 40mm in height. The normal load is first applied to the upper block before the shear load is initiated. The time step is set in order to have a horizontal shear velocity of 4.139 x $10^{-}8$ m/time step. The model tests shear deformation/stiffness for saw-tooth triangular joints of dilation (i) at 15, 25, and 35 degrees, which are all simulated for an initial normal load of 1, 2, 3, and 5 MPa. These normal stress levels are all in CNL conditions. The simulations are based on a "Bond removal approach", where fractures are simulated through the failure or detachment of these bonds based on certain criteria or conditions. When the defined criteria are satisfied, the bonds between particles are removed, thereby simulating the separation of cohesive forces. In order to observe bond removal in this particular software, planar joints are also simulated in a sensitivity study.

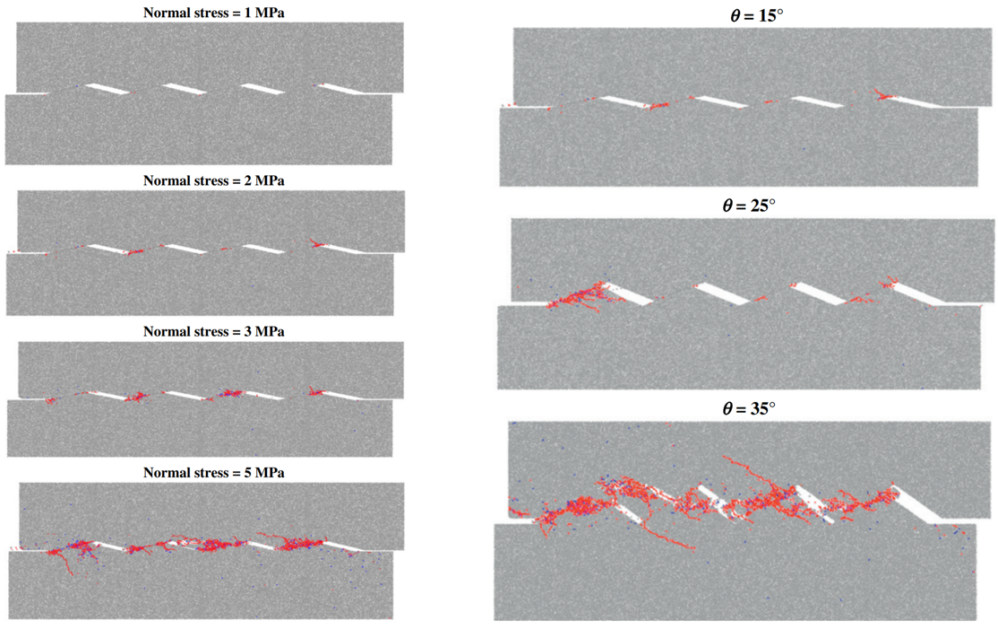

Figure 2.12: Indication of fracturing during shear simulations at various normal loads and dilation angle of saw-tooth triangular asperities

This numerical study consisted of a sensitivity study using planar joints while analyzing the shear results using different friction parameters from 0.005 to 0.15 under $P_i = 1MPa$. The planar joint model initially produced unrealistic results, as the peak shear strength increased with a reduced frictional coefficient. The error source was the model interpretation having the micro-scale roughness with circular asperities getting interlocked in during the shear stage. This is not a relevant issue when using ABAQUS, where tangential surface interaction may use frictional coefficient as a direct input parameter. However, it does highlight the value of conducting a sensitivity study to map out issues for certain aspects of the model.

Using the Patton model for triangular asperities (Patton 1966), good agreement was

found between the results of different angles and normal loads compared to experimental studies.

Another aspect that was researched is the use of peak shear strength envelope using the bond removal method with a small degree of friction. The bond removal method was unable to realistically model the shear displacement for both the planar and angled surfaces. For the planar joints, it was expected that the shear-normal stress relation would follow the Mohr-coulomb criterion (equation 2.1); however, bi-linear relation was shown for both triangular and planar joints. Results showed an overestimated cohesion at low normal stress and a significant difference in peak shear strength for high normal stresses. For the smooth joint model, the particle bonds were defined so that all contact points between the mated walls may overlap and pass through each other. In this way, the concentrated "hitch" points that were problematic in the bond removal model were avoided.

From the sensitivity study of the "smooth joint model", it was shown that the model was able to realistically simulate shear stiffness only to the point of horizontal displacement reaching the minimal particle diameter at 0.3 mm. The method was therefore concluded as unsuccessful.

The Shear box genesis approach that was finally deemed successful consisted of surface generation, application of parallel bonds, application of smooth joints, and removal of floaters, all at individual steps. Validation was done according to procedures explained in S.C Bandis et al. 1983.

As mentioned, the shear strength was tested for asperities of 15°, 25°, and 35°, with results plotted over normal stress and compared to the Patton model in equation 2.2(Patton 1966) and Ladaniy and Archambault model in equation 2.16 (Ladanyi et al. 1969). From RE Goodman 1974, it's suggested that transition pressure is used in the two mentioned methods.

When using this study for comparison, some things are worth taking note of:

- This study makes use of the secant shear stiffness method from R.E Goodman et al. 1968 and does not cite any non-linear stiffness criteria.
- For CNL conditions, smaller joints generally showed rapid drops in post-peak shear strength due to brittle failure characteristics. This was especially apparent for high JRCs. Larger joints are, to a larger degree, affected by ductile failure characteristics.
- Shear stiffness increased very little from 30% of UCS normal load and higher. Shear stiffness approached 0 hyperbolic as the joint length increased.

Both the planar and saw-tooth models used in this study can be replicated and used in a FEM model can be done in order to adjust curves. In terms of stiffness and shear criterion, this study only cites

Following up on Bahaaddini et al. 2013, Liu et al. 2020 conducted a similar study while focusing on the scaling effect, while the parallel bond and the smooth joint model are

still implemented. Shear tests are simulated for CND, CNS, and CNL conditions.

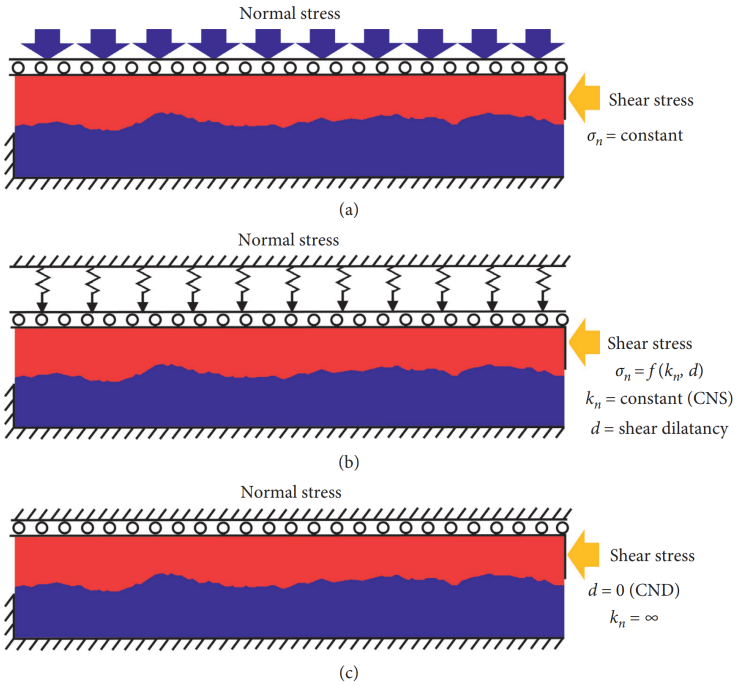

Figure 2.13: Numerical joint closure. (a) Top view of lattice-grid cylindrical asperities. (b) Side view of initial asperities before normal load. (c) asperities after applied normal load (L. Wang et al. 2016)

This study also uses the PDF2D software, similar to Bahaaddini et al. 2013. In this software, the intact rock is represented by the assembly of particles, which are bonded together. The damage process in rock failure and plastic deformation is represented by the removal of these bonds. In addition to the macro-parameters (E-modulus, K_n, K_s, etc.), a parallel-bonded model is used, which requires the input of micro-parameters in addition to the general material parameters used in FEM modeling. This can be explained as a set of elastic springs over the rectangular cross-section with constant bonds of normal- and shear stiffness that are uniformly distributed in the mesh (Lai et al. 2007). These parameters include bond stiffness ratio (K_n/K_s), which also must be defined for particle bond parameters ($\overline{K_n}/\overline{K_s}$). Likewise, other parallel bond parameters must be defined for Young's modulus, UCS, and cohesion.

When addressing the scaling effect, the above-mentioned parameters were extracted from physical shear and UCS tests using an artificial joint from a slab of concrete. All joint lengths (100, 200, etc. mm) were simulated under CNL, CNS, and CND conditions with three levels of normal stress, at 10%, 30%, and 50% UCS, respectively. The models also focus on higher JRCs as smooth joints. The shear strength of smoother joints is less affected by failure in asperities.

Four main indexes were observed; Peak shear strength τ_{peak}, peak shear displacement ϕ_{peak}, peak shear displacement d_{peak} and shear stiffness k_s.

In the case of shear stiffness. The scaling effect was apparent as the stiffness had a

hyperbolic approach to zero with longer joints. This is due to the lower τ_{peak} and higher ϕ_{peak}.

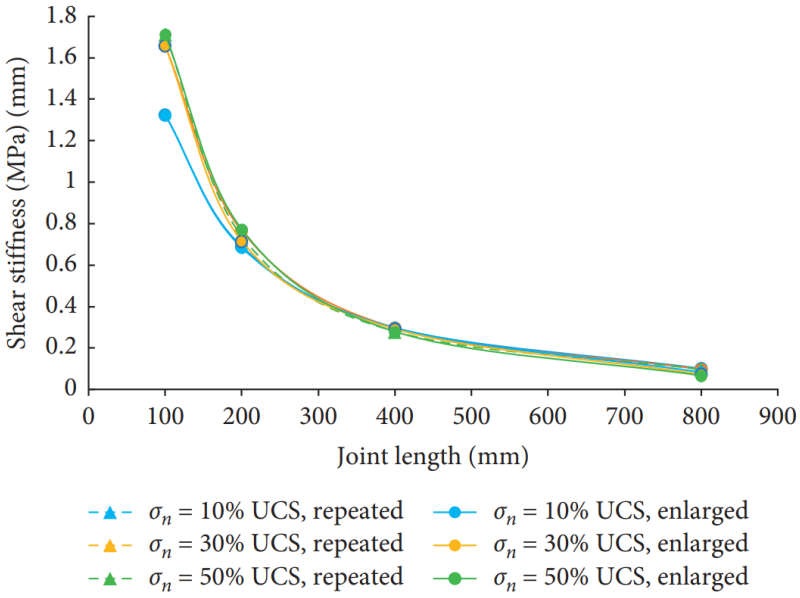

Figure 2.14: Numerical joint closure. (a) Top view of lattice-grid cylindrical asperities. (b) Side view of initial asperities before normal load. (c) asperities after applied normal load (L. Wang et al. 2016)

2.8 Modeling in ABAQUS

Numerical modeling is commonly used in engineering geology for purposes like stability analysis in excavations, the effect of rock support, etc. For the above-mentioned purposes, software like Rocscience RS2, GeoSys, Leapfrog, etc., is typically used, as these contain predefined, user-friendly modeling tools.

For the modeling purposes in this paper, the model development requires very specific handling of contact interaction which goes beyond what is possible in Rocscience software. ABAQUS provides very detailed handling of such interactions while also being user-friendly and suited for engineering students who are previously unfamiliar with the program.

A majority of calculations in this work are in relation to stress and displacement. In finite element reaction forces (RF) are calculated for each node, including the x- and y-components. When replicating normal loads and direct shear tests, the normal and shear stresses are measured for the entire sample. In order to find these values in the post-processing of the numerical models. The total stress of the sample in one direction can be calculated by summarizing the reaction forces along the top boundary of a sample and dividing it by the total area.

In ABAQUS post-processing, the 1 and 2 directions describe the x- and y-direction in the model, respectively. It's important to note that ABAQUS does not use pre-determined

units. For the sake of this work, SI(mm) is used due to the scale of the samples in the simulation.

As mentioned, one problem relating to the challenge of repeatability of shear tests of rock lies with how it is impossible to repeat a test with the exact same sample characteristics. One method to overcome this in modeling is to select material that can be easily handled and reproduced in the verification process Shrivastava et al. 2015. For example, Plaster of Paris, which is an easily reproduced material used by Shrivastava et al. 2015 to stimulate soft rock.

3 Model development for numerical shear tests

Using ABAQUS CAE it is possible to create specific situations of rock mass modeling using plastic material definition and fracture criteria that are common in engineering geology. The ABAQUS software also has the advantage of being relatively user-friendly, and commercial accessibility, making the work done in this thesis convenient to build upon in future work. This has been used in prior work to successfully model joint closure under normal load with both plastic and elastic material parameters, giving qualitatively comparable results to experimental research (JianPing et al. 2015) and (Lavrov 2017).

As ABAQUS does not use pre-defined units, commitment must be made to a unit system. At the scale of joint shear tests, the SI(mm) unit system is the most sensible and compares best to similar research. All results in this work will be using the SI (mm) unit system (Table 3.1).

Table 3.1: SI and SI(mm) unit system

	SI	SI(mm)
Length	m	mm
Force	N	N
Mass	kg	tonne
Time	s	s
Pressure	Pa (N/m)	MPa
Energy	J	mJ
Density	kg/m^3	$tonne/mm^3$

As discussed in the theory section, the shear stress-displacement relation is dominated by plastic behavior after the peak shear stress is reached due to the crushing of asperities (S.C Bandis et al. 1983). In the early phase of the modeling work, only elastic material parameters are defined. To make the process of making the physical aspects of the actual direct shear test, including the normal load step, correct as possible. This also makes the process of finding issues relating to convergence and some obvious unrealistic output.

With calibrated models, it's desired to achieve similar results as studies using similar set-ups and input parameters. Modeling the shear blocks with triangular saw-tooth asperities and comparing model results to other numerical studies of rock joint behavior is possible. Doing this, parts geometry is easy to replicate and can be created using ABAQUS sketching tools.

Other numerical studies discussed use CNL, CNS, and CND conditions interactively. Both for the sake of a sensitivity study and the work on shear models, CNL and CND conditions can be defined using either load or displacement as the factor for normal and shear stress. Since both of these are simple to recreate the boundary conditions for, both of them are researched in detail for the shear test.

In addition to the sensitivity study and the tests themselves, the scaling effect is also researched under CND conditions.

3.1 Sensitivity study of normal stress models

A two-part contact model is made using three different surface geometries to observe convergence as well as the validity of stress-displacement using elastic material parameters. The setup for the constant normal load (CNL) and constant normal displacement (CND) is shown in Figure 3.1. For the normal stress model, the terms CNL and CND are used for weather stress is determined by input load or displacement, respectively. The two surface geometries, which do not include flat-surface joints, are set to represent a rough joint surface approximately. For the CND conditions, one challenge is reaching a desired level of initial normal stress, P_i, by adjusting the normal displacement of the top block. S.C Bandis et al. 1983 provides some insight into the relations of maximum aperture and maximum joint closure for mismatched joints, which in this case is relevant for the hand-drawn joint, where the contact area between the joint surfaces changes during normal load. For the remaining joints, the linear stress-displacement relations are simple to calculate, as the contact area remains the same. As a starting point, the displacement is set to $0.6mm$ for CND conditions. For the CNL conditions, the initial normal load is defined directly.

The three geometries used are as follows:

- Hand-drawn mismatched asperities
- $0° - 0°$ flat surface
- $15° - 15°$ saw-tooth

These surface geometries were used interactively in the sensitivity study to identify convergence issues. $0° - 0°$ flat surface is only used in sensitivity studies and not in further sections.

3.2 Numerical setup

The reviewed numerical studies vary in how boundary conditions are defined. For the CNL model, the bottom part of the bottom block is fixed. Figure 3.1 shows the setup for BCs for the hand-drawn irregular joint. The same BCs apply to the other two geometries.

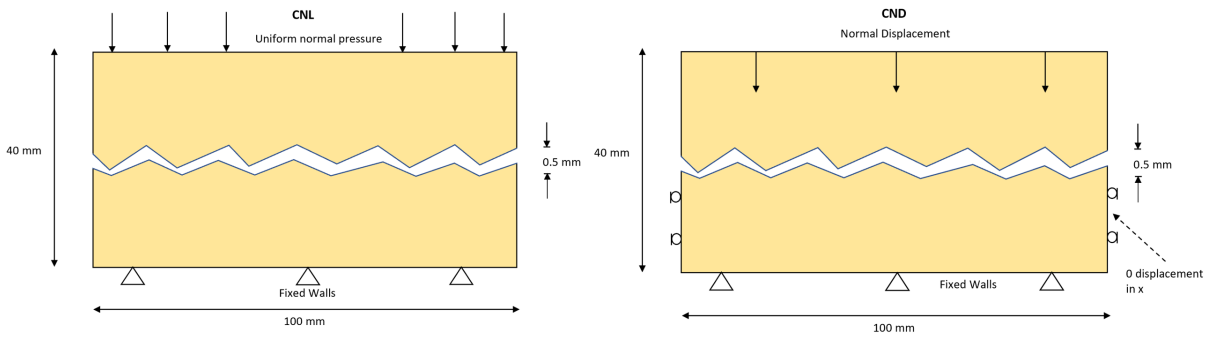

Figure 3.1: Initial setup for CNL and CND first load step

Material parameters are defined as shown in Table 3.2. For comparison, these are set to

be the same as in Shrivastava et al. 2015. Time increment is at this stage not adjusted as displacement velocity will not affect the results for elastic models. The load/displacement step is separated into multiple time increments, making it possible to plot the stress-displacement curve. This was set to 5 seconds by default. For a contact model, it's also necessary to define the interaction properties of the surface contact. At this stage, these properties were defined as frictionless, hard contact.

Stress is calculated by summarizing reaction forces registered at a path that is set along the bottom edge of the bottom block. The sum of the reaction forces RF2, we find the total normal stress of the test, for the CNL models displacement is tracked using constraints. By defining a coupling constraint along the top surface of the top block, allowing displacement in all directions, a reference point can be used to represent the output of the entire top surface. For CND models, this has to be done by using a path along the top part of the top block in post-processing, extracting the displacement data, and calculating the average normal displacement.

Table 3.2: Properties for the first test models

Property	**Value**	**Unit**
Material Parameters		
Density	2.6 x 10^{-9}	tonne/mm^3
Poisson's ratio	0.3	
Young's Modulus	4.2	GPa
Surface interaction		
Frictional formulation	Frictionless	
Pressure-overclosure	Hard contact	

Another goal of the first model is to test convergence for the contact model and attempt to measure normal deformation qualitatively. One challenge in this particular model lies in defining boundary conditions and contact surfaces.

3.2.1 Mesh

Another factor to be evaluated in the model development stage is the choice of the mesh element type. Generally, the choice between plane stress and plane strain depends on the type of problem one is trying to solve. In-plane-strain mesh, the material is constrained in one dimension and can deform freely in the other two dimensions (x- and y-direction). Commonly plane strain is assumed when the modeling structure is subjected to large deformations in the plane. Plane stress restricts the out-of-plane deformation to zero. This is used when assuming out-of-plane deformation to be neglectable. As saw-tooth models are used, the geometry is identical out-of-plane to the 2D sketch. When comparing to the use of JRC as surface geometry, variations out-of-plane is assumed to be similar and should, in theory, not affect the validity of the results of a 2D model while making

similar assumptions as in Bahaaddini et al. 2013 and Liu et al. 2020. Also, in the models where plasticity is added to material parameters, 2D models will only converge if plane strain elements are used. The mesh element type is therefore set to plane strain.

For mesh geometry, quad element shape is standard in ABAQUS CAE and has also been used in similar studies. JianPing et al. 2015 is one example. As a starting point for the sensitivity study, this was used here as well. The seeding size is set to 1 for all parts to ensure a convenient solving speed for the model, as well as having one element per mm of the entire shell element. The quad mesh for the bottom part of the 15-degree saw-tooth model is shown in Figure 3.2.

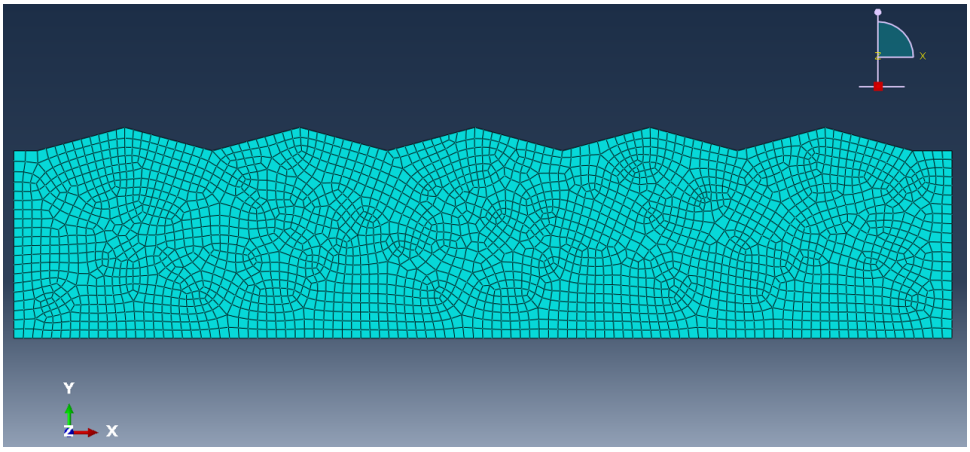

Figure 3.2: Quad mesh with seeding set to 1

3.2.2 Interaction

For the contact model, surface interaction requires defining tangential and normal behavior. In other numerical studies, both frictionless behavior and penalty (friction coefficient) are used. For the initial models, frictionless behavior is chosen to limit potential sources of convergence errors.

For surface-to-surface contact, the matched surfaces need to be defined as slave surfaces or master surface. The master surface is typically associated with that has controlling behavior in the interaction or the initiated movement. The slave surface is associated with the surface that responds to the imposed conditions. In this case, the movement is initiated through the top part, while the resulting forces are registered at the bottom part. For the mentioned reasons, the surface-to-surface contact was set with the top part as the master surface and the bottom part as the slave surface (Figure 3.3).

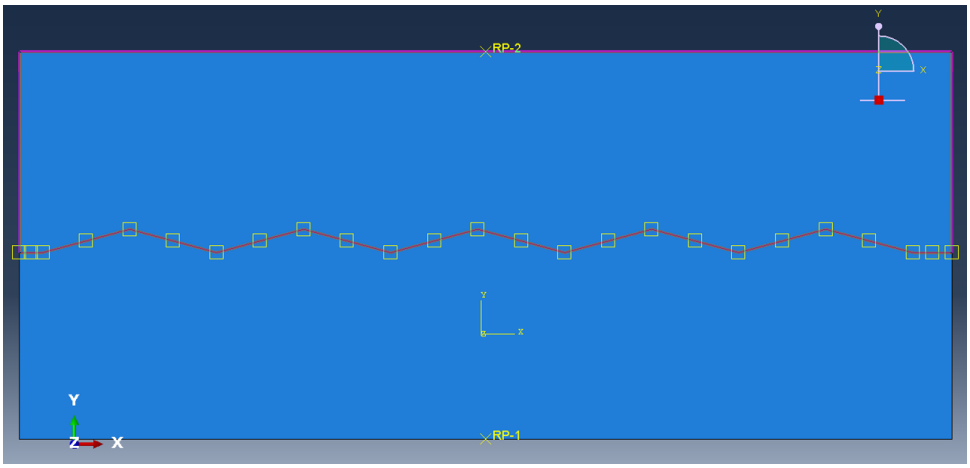

Figure 3.3: Interaction with master- and slave surface

3.2.3 Post-processing

After the model is successfully run, results are gathered in post-processing. For this study, the main aspects of interest are:

1. Shear/normal displacement for the top block
2. Shear/normal total stress gathered from reaction forces from the bottom block.

As part of the sensitivity study, multiple ways of finding the desired results were attempted, including defining History Output for each model before simulation. The most successful method was using paths along the bottom and top edges of the respective blocks. The path along the bottom part of the bottom block (Figure 3.3) was used for registering normal and shear reaction forces. This made the replicability of every simulation fairly simplistic. With a set path on both blocks, "XYData" lets one choose the source of data, with "Path" as one of the options. From there, it's possible to select "Include all elements along path". Since BCs are defined to only have the bottom edge pinned, all reaction forces for registration of the total stress of the model are included in these elements.

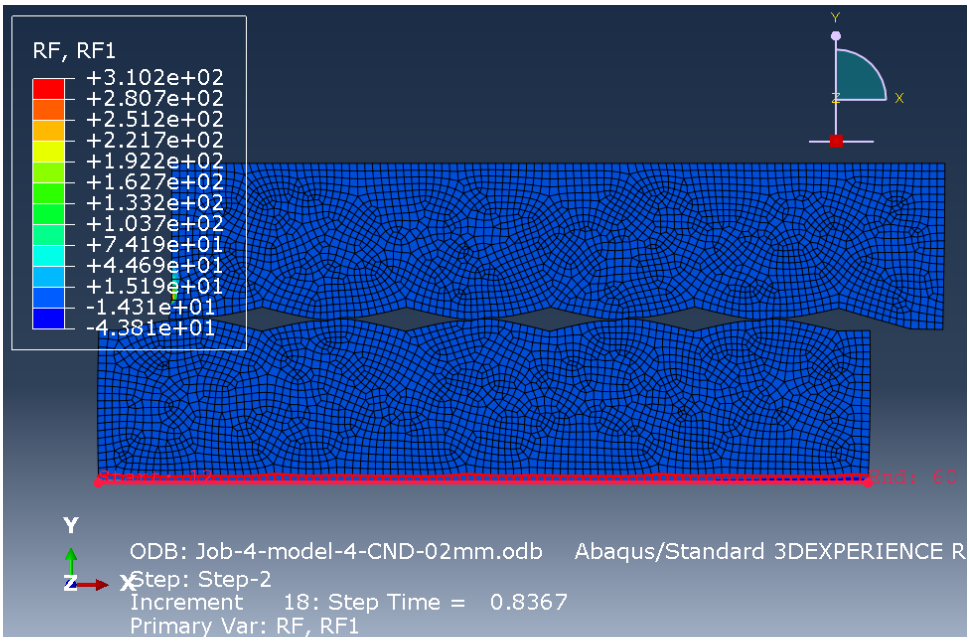

Figure 3.4: Path along the bottom part of the bottom block with all adjacent elements included used for exporting reaction forces

3.3 Normal closure with different surface geometries

With some tweaking of boundary conditions between each step, all models were able to converge for one displacement or load step. The irregular joint surfaces from the hand-drawn model had a lot more difficulty converging compared to the two others. In the early stage of the model work, it was clear that contact models aborted early when angles were moved into flat edges. When experimenting with more rounded asperities, it was possible to achieve higher normal displacement. For that reason, the flat surface joint and completely matched saw-tooth joint were introduced.

3.3.1 Flat surface joint

This model was mainly used to map out convergence issues while also confirming realistic stress-displacement output.

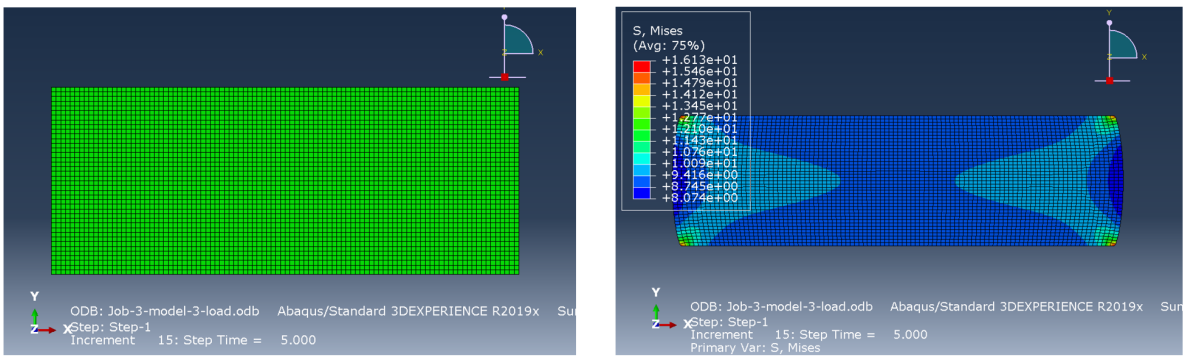

Figure 3.5: Model setup and stress distribution for elastic flat surface model

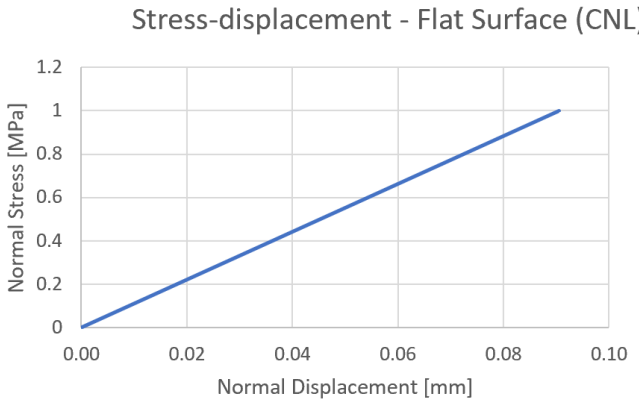

Figure 3.6: Stress-strain output for flat surface elastic model

Results show completely linear stress-strain relations, as expected when contact surfaces are constant. Stress distribution had the highest stress levels diagonally through the parts, which may compare to the fracture angle in UCS-test.

3.3.2 Matched saw-tooth joint

With this joint geometry, which resembles an interlocked joint with perfectly matched joint surfaces, convergence was achieved with similar deformation as the flat-surface model. Stress-displacement relation and stress distribution proved to be similar, even with some sliding occurring. With only normal load/displacement, it had minimal to no effect on results at this stage.

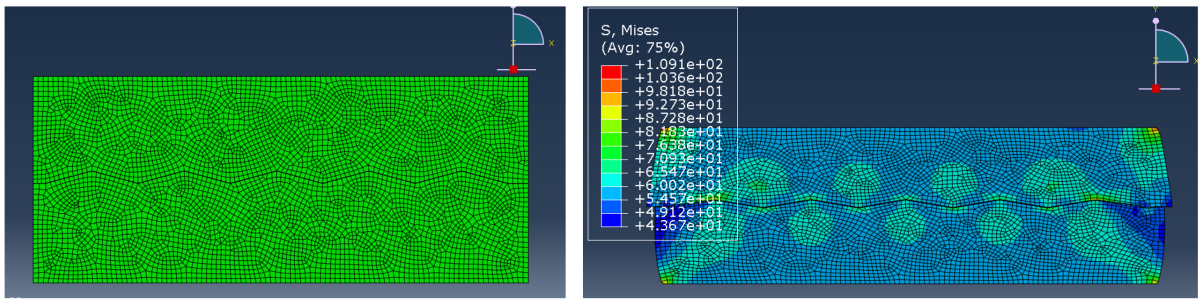

Figure 3.7: Model setup for elastic 15 deg saw-tooth model

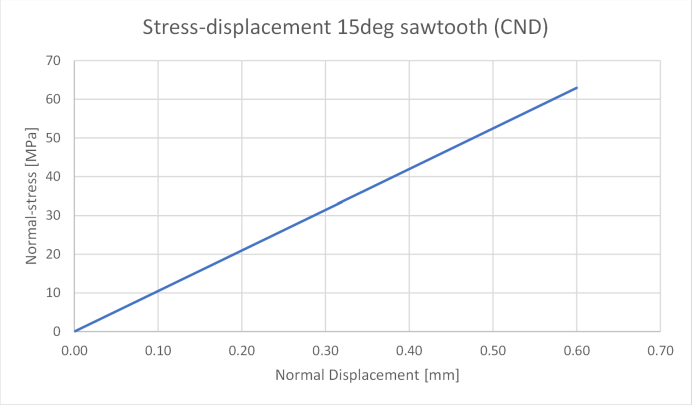

Figure 3.8: Stress-displacement of mismatched hand-drawn asperities under constant normal displacement

From the results plod (Figure 3.8). A higher initial normal displacement was attempted and converged. However, the normal stiffness was unchanged at 105 MPa/mm.

3.3.3 Hand-drawn joint surface:

Compared to the two other surface geometries, this model would abort before 0.2 mm normal displacement. At that point, only three asperities had reached contact (Figure 3.9). When using normal load instead of displacement, the model was unable to converge at all.

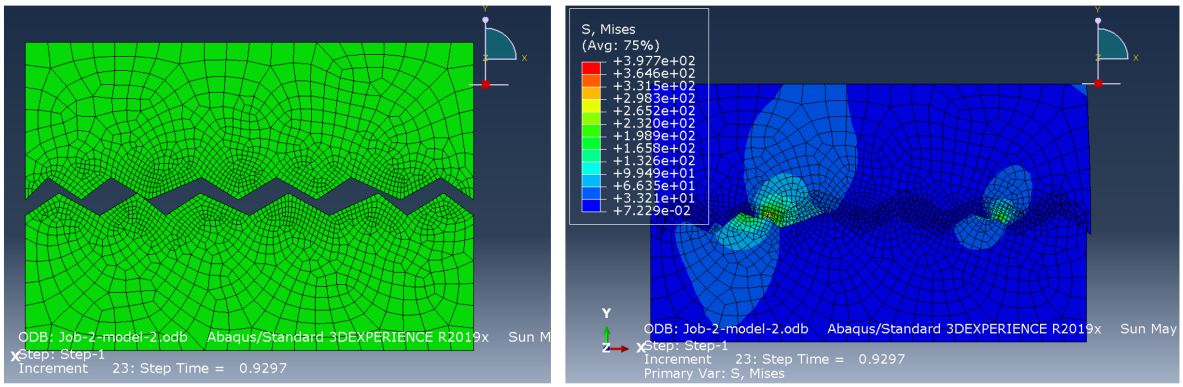

Figure 3.9: Stress magnitude of last converged increment of normal displacement

The reason for convergence issues is not completely certain. However, using the last converged increment, it was possible to extract the necessary data to create a stress-displacement curve (Figure 3.10)

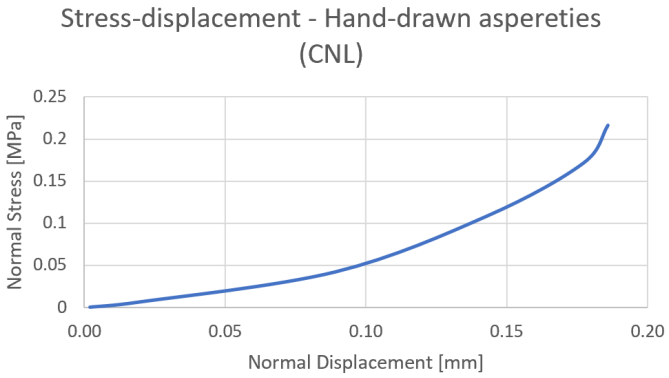

Figure 3.10: Stress-displacement of mismatched hand-drawn asperities under linear normal displacement

With the convergence issues with the current model, introducing a second step for shear movement was impossible. However, the exported results from reaction forces did resemble the hyperbolic stress-displacement curve similar to Figure 2.3 (S.C Bandis et al. 1983) as the curve was seemingly approaching a constant displacement for higher levels of stress.

3.4 Shear without normal load

Continuing with the $15° - 15°$ saw-tooth model, shear stress-displacement was observed under constant normal displacement, which was unchanged from zero after the initial stage. With CNL conditions, the model is more likely to have sliding being the main factor for displacement. From Shrivastava et al. 2015, the shear process should have an increase in stiffness until the point of the asperity peaks crossing each other for the mated walls. For this setup, that will occur at 9.33 mm shear displacement when the asperity tips reach each other.

With no normal displacement or pressure applied, horizontal displacement is set as BCs for both sides of the top block. The choice of using the block walls as opposed to the top was to limit deformation above the triangular asperities. Resulting shear-stress-displacement plot (Figure 3.11). This was the result using 3mm horizontal displacement.

When increasing the displacement, convergence stopped when the horizontal displacement reached 8.66 mm.

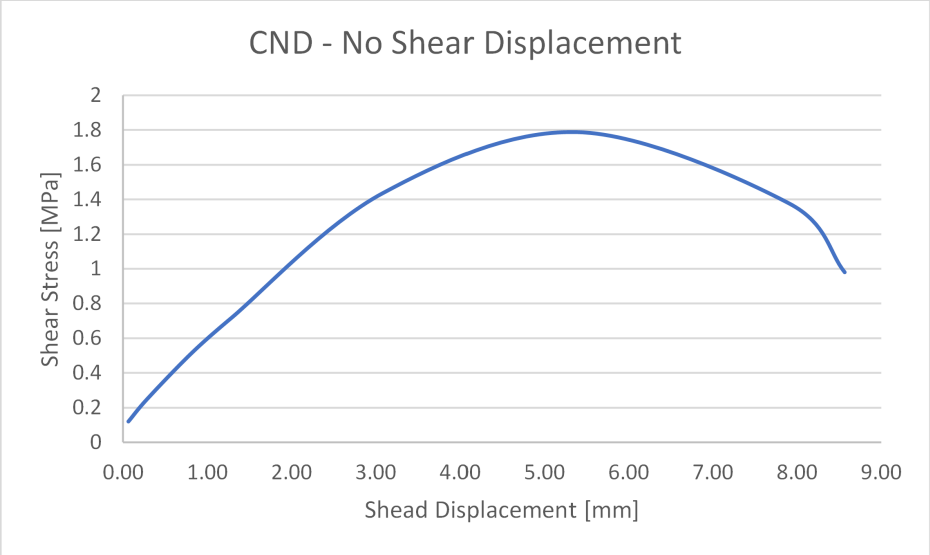

Figure 3.11: Stress-strain plot for elastic shear of 15 deg. Saw-tooth asperities until last converged increment

Plotting the stress-displacement of the CND model (Figure 3.11) shows a curved plot with a peak at approximately 0.65 mm horizontal displacement.

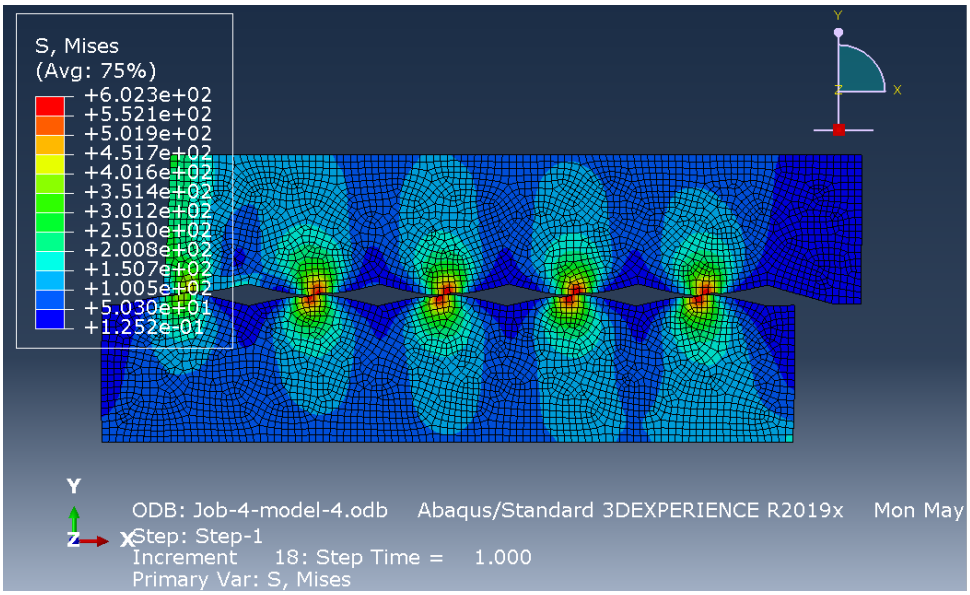

Figure 3.12: Stress magnitude at last converged increment of CND Elastic shear model

Figure 3.12 shows the stress distribution (mises) at the last converged increment, with the highest measured stress at approximately 600MPa at the tip of the asperities. At this point, the sliding stage described in Liu et al. 2020 (Figure 2.8) is finished, and asperity fracturing is starting.

In order to better understand the effect of interaction properties, the tangential contact was changed from "frictionless" to "rough". The stress displacement relation did again

prove to be perfectly linear. The model was, with this tweak, unable to converge for the same horizontal displacement and could now only converge for 3.6 mm. When experimenting with a horizontal load instead of displacement, the model crashed after achieving a horizontal displacement of approximately three micro-meters (Figure 3.13)

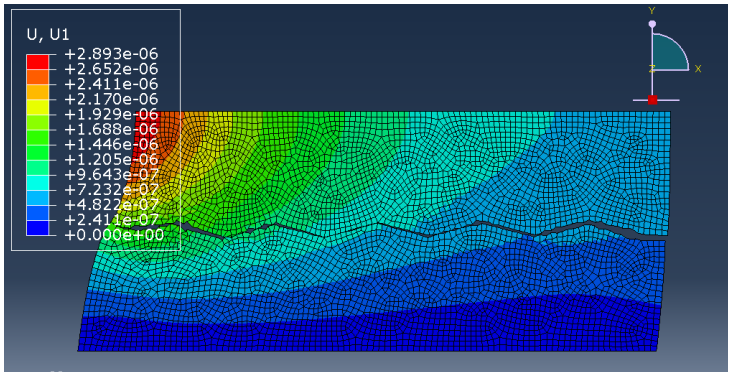

Figure 3.13: Shear displacement at last converged increment of CND Elastic shear model

Since the surfaces were in 100% contact from the initial stage, the total sample would behave the same as one solid block when exposed to stress.

3.4.1 Boundary Conditions for elastic 2D models

When reviewing different shear tests in the literature, multiple different setups were used in how the sample parts were connected to the shear box. In that context, it seemed relevant to experiment with different boundary conditions along the walls of the sample, given that some shear tests have the shear box confining more of the sample walls, which will to a lesser degree, allow deformation in the sample part that did not directly relate to the joint asperities.

This process created difficulties in terms of applying multiple steps for some part geometries, as the model would not converge unless removing the confining zero-displacement in a horizontal direction after the first step. When removed, the stress levels were visibly reduced in the horizontal direction (Figure 3.14). In addition to this, these boundary conditions made post-processing more challenging, as RFs could no longer be collected by using a path along the bottom block.

- Step 1: initial boundary conditions are defined in order to initiate normal displacement. having the bottom part of the bottom block pinned in all directions while having zero displacements in the x-direction for the confining walls and top block. The joint surface and the first 4mm of the top and bottom wall are only defined to have 0 displacements in z (into the plane). Y-displacement is set to -1mm.
- Step 2: Walls and the top of the upper block are no longer set to zero displacement in the x-direction, releasing some of the pressure.
- Step 3: Displacement set to 1 mm in x directions for both walls on the top block

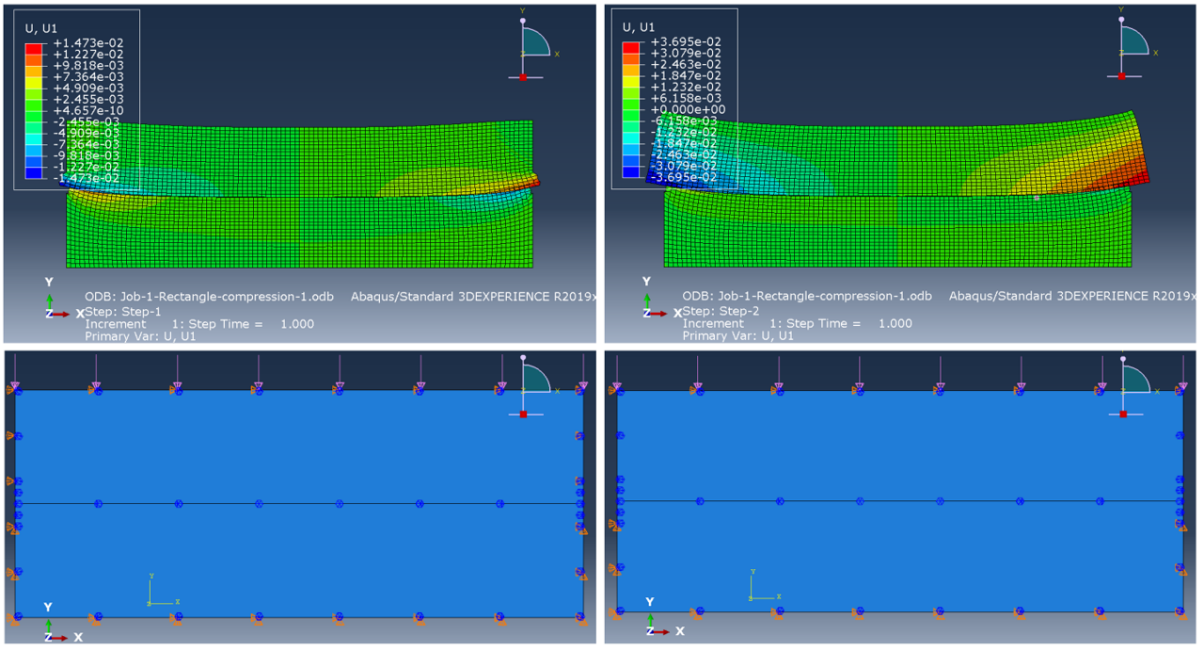

Figure 3.14: Boundary conditions for flat surface model

With some of the part geometries used in the sensitivity studies, this extra step proved to be unnecessary as it both created an extra source of error, as well as having little to no effect on the end results.

3.4.2 CNL and CND conditions

During work in the prior section, this caused a lot of issues when trying to get model convergence using load for 2-part models, at which point it was decided to proceed only using CND models. However, it was discovered that the issue with load input did not occur when the two parts were in contact with the initial step. As implied in Liu et al. 2020, CNL models are more realistic in low-stress situations, giving more incentive to making these models work in trying to replicate direct shear tests, being able to control the normal stress level before the shear displacement makes the numerical work significantly easier. This is further elaborated in section 4.2.

It was then decided to proceed with only having the bottom surface of the bottom block pinned while allowing all degrees of freedom for the remaining surfaces.

In the 3rd step, it's preferred to have shear displacement initiated. Ideally, the first two steps have then reached the desired level of normal load.

3.4.3 Sensitivity studies - results

Achieving convergence proved to be more challenging than expected, especially using load instead of using displacement as a boundary condition. One of the main factors for this seemed to be the stress distribution caused by the sharper asperity angles. From the $15° - 15°$ saw-tooth model, having complete surface contact between the two parts made convergence easy to achieve both for load and displacement models.

The stress-displacement results in terms of curve shape were logical and did, to some extent, resemble the S.C Bandis et al. 1983 experimental results for interlocked and mismatched joints under normal pressure. Even with elastic parameters, the increased amount of contact points during joint closure lead to a hyperbolic relation. For the matched-15degree saw-tooth model, the stress-displacement relation was completely linear, similar to the flat surface model. This is expected when no plastic deformation occurs, and the contact between the surfaces remains the same throughout the whole displacement process.

Compared to the PCF2D model in Bahaaddini et al. 2013, stress levels were not the same when using similar output parameters that were possible to use directly in ABAQUS.

3.5 Elastic CND model - Shear under normal displacement

Still using elastic material parameters using the 15-degree saw-tooth triangular asperities to do the following:

- Converge for 2-step analysis with normal pressure followed by shear
- Qualitatively replicate a shear stress-shear displacement plot with elastic properties
- Observe the effect of individual model aspects

The reason for using the 15-degree saw-tooth joint is mainly for comparison reasons. From Bahaaddini et al. 2013, this joint geometry gave the least amount of plastic behavior and fractures compared to triangular joints with higher dilation angles for better comparison. As mentioned, in the PCD2D used in the model, fractures are simulated using parallel bonds. As the FEM model used in this section still only contains elastic properties, this is still not a relevant comparison issue.

As mentioned, one of the challenges with using CND is to achieve the initial normal load before shear displacement. This linear relation, as shown in Figure 2.8 can provide the normal displacement for the P_i values used in Bahaaddini et al. 2013. This assumes complete surface contact from the initial stage.

While using frictionless tangential interaction, simulation of shear stress-displacement was observed under different levels of initial normal displacement.

First, the model is tested for normal displacement in order to pinpoint what normal displacements are needed to achieve desired normal stress levels at 1 MPa, 2 MPa, 3 MPa, and 5 MPa. The model is run with one step at normal displacement set to 3mm. RF2s are measured and summarised along the bottom path like in Figure 3.4. Results for initial normal stress are shown in Table 3.3.

Table 3.3: Normal load and displacement for 15-degree elastic saw-tooth model

P_i [MPa]	$U1_i$[mm]
1.0	0.01
2.3	0.02
5.1	0.05
10.02	0.09
20.01	0.18

Results from Table 3.3, this approximately resembles elastic deformation for intact rock.

With these results, we have that for U2 =0.01 mm, σ_n approx = 1 MPa. Using this, shear stress-displacement was tested for initial normal displacement 0.01, 0.02, 0.03, and 0.05. Horizontal displacement is set to asperity length at 9.33 to ensure the model runs to the last converged increment. The last converged increment was at an average U1 of 0.89 mm.

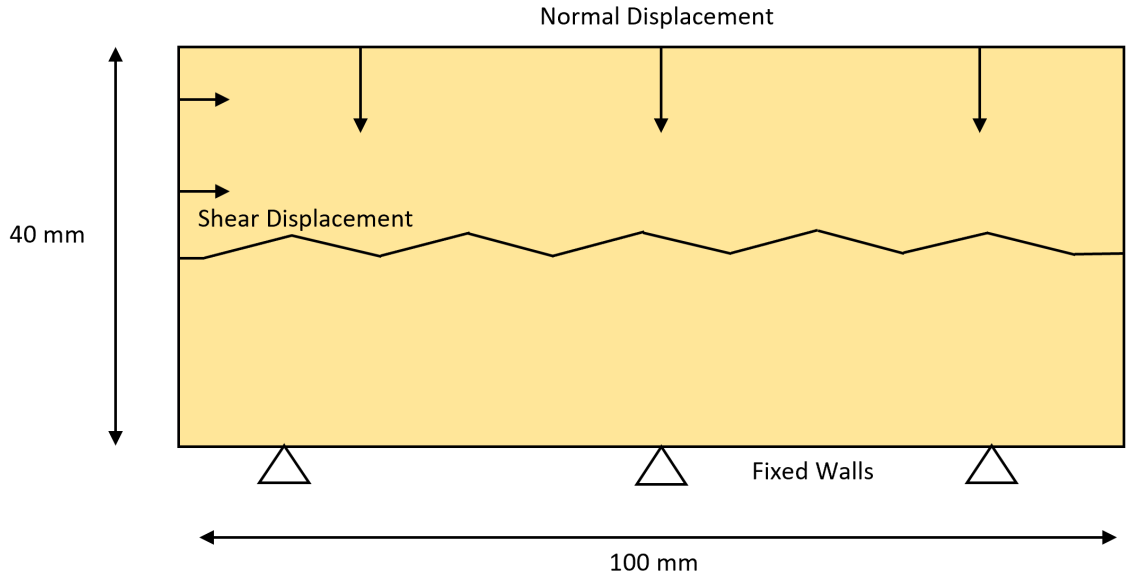

Figure 3.15: Setup for elastic CND 2-step normal and shear displacement

The step for step setup for the CND model was as follows:

- Step-1: initial boundary conditions are defined in order to initiate normal displacement. This follows the same setup as the prior CND model, having the bottom part of the bottom block pinned in all directions while having 0 displacements in the x direction for the confining walls and top block. The joint surface and the first 4mm of the top and bottom wall are only defined to have zero displacement
- Step-2: Walls and the top of the upper block are no longer set to 0 displacements in the x-direction, reducing some stress

- Step-3: Displacement set in the x-direction, initially set to 10 mm as the model is aborted before this displacement is reached

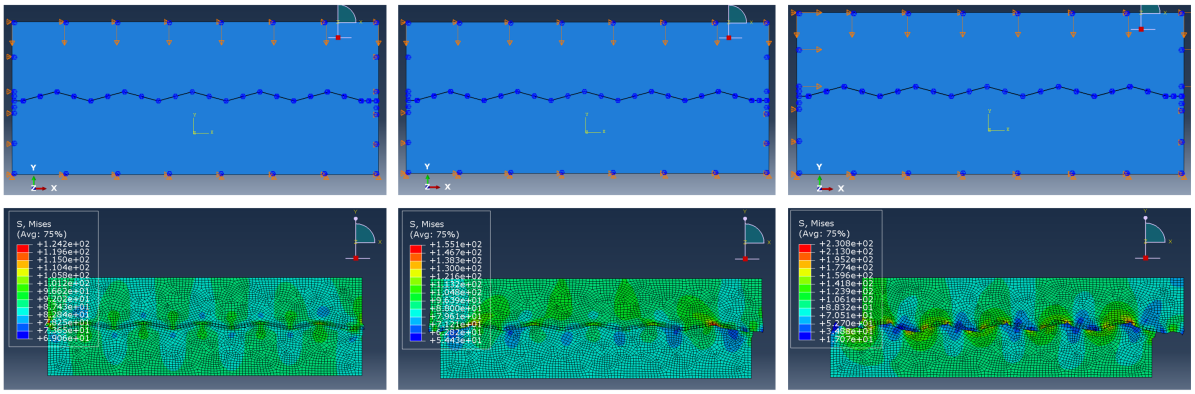

Figure 3.16: Boundary condition setup for CND model

As explained in the prior section, step-2 proved to be unnecessary.

Similar to the Bahaaddini et al. 2013 study. Normal displacement is set to have similar initial normal pressure at 1, 2, 3, and 5 MPa. The stress-displacement curve is plotted for each simulation.

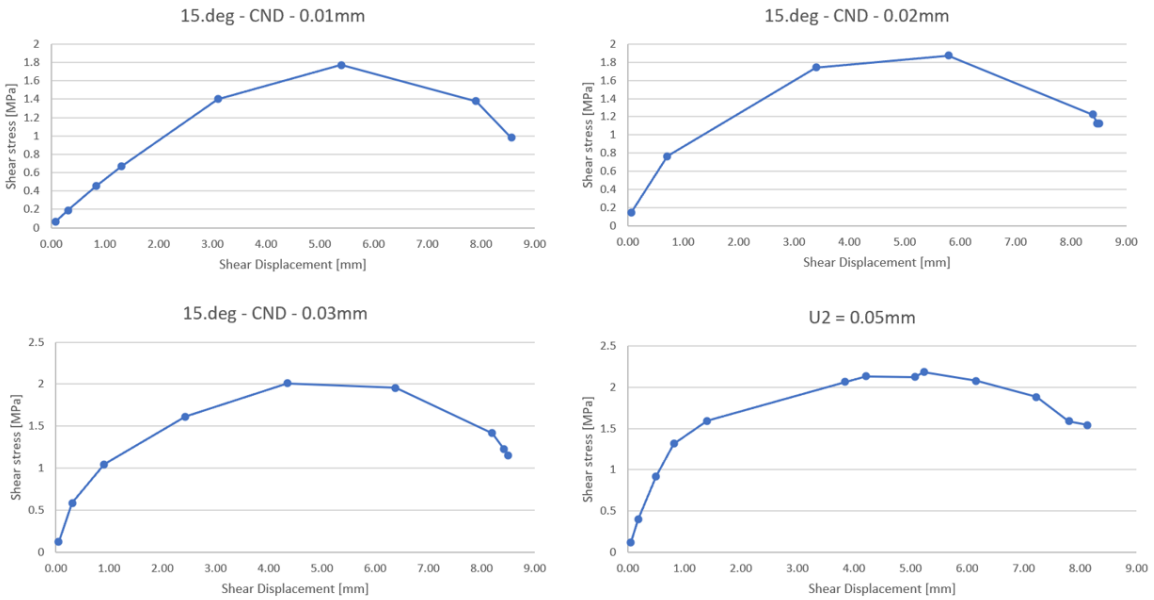

Figure 3.17: Shear-displacement plot elastic CND for normal displacement (0.01mm, 0.02mm, 0.03mm, and 0.05mm)

From viewing the plots in Figure 3.17 and 3.18, it's clear that the peak shear stress increase with higher levels of normal displacement. This compares well to other experimental and numerical studies. Other than that, the 0.01 mm and 0.05 mm models have

a clear linear increase from zero before shear stress has reached 50 % of its peak. This is not the case for the 0.02 and 0.03 models.

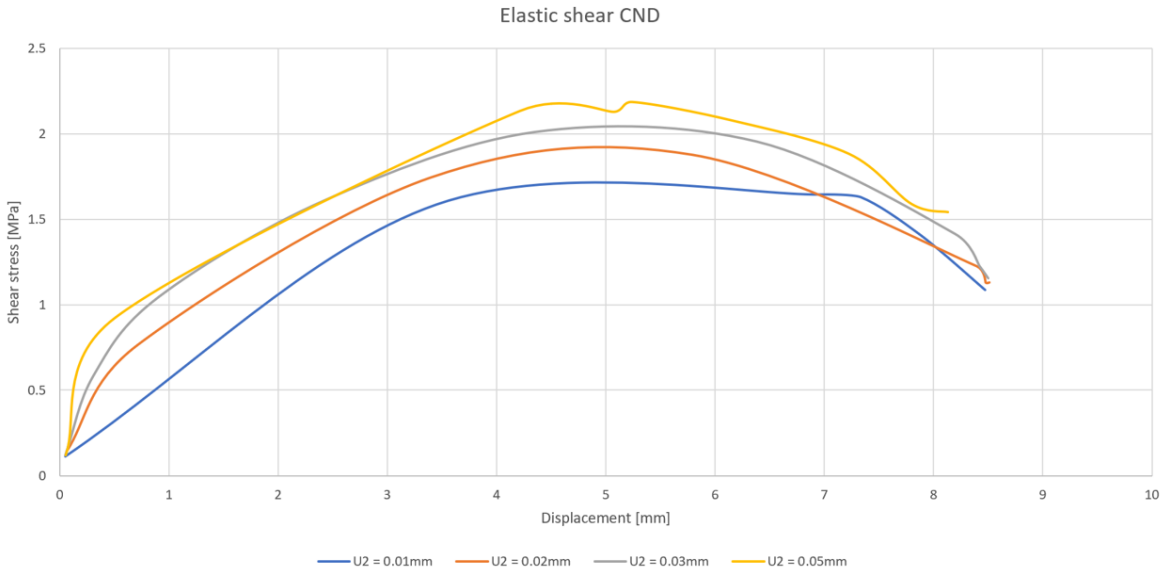

Figure 3.18: Summary of results from elastic CND models

By using only elastic material parameters and CND conditions, some of the trends from a physical direct shear test under normal displacement were shown. Most importantly, how peak shear increases with increased normal stiffness (S.C Bandis et al. 1983). The model shows a realistic relation when sliding and shearing are the primary displacement factors (Figure 2.8) (N.R Barton 2013). From other numerical studies, the shear strength increases with normal stress until peak shear stress is reached. Plastic behavior starts after peak shear is reached. In the case of this model, regardless of initial normal displacement, peak shear strength is reached approximately at 4-5 mm horizontal displacement. Considering the horizontal width of the triangular asperities is at 9.33mm, this is at approximately 43% - 54% of the peak asperity height, whereas according to Shrivastava et al. 2015 experimental studies using 15.degree triangular asperities, the same relation was shown when using similarly sized asperities Figure 8. The reduction in shear stress from this point is attributed to asperity crushing, which does not apply to this current elastic model.

Table 3.4: Results of CND at different initial normal displacement

U_n [mm]	τ_{peak} [MPa]	$\sigma_{n,i}$ [MPa]	$U1$ at peak shear [mm]	$\sigma_{n,peak}$ [MPa]
0.01	1.77	1.016	5.24	100.43
0.02	1.88	2.032	4.35	101.01
0.03	2.01	3.047	5.79	101.58
0.05	2.18	5.079	4.81	102.72

Table 3.4 shows the results of elastic CND plots using different normal displacement (U_n),

with max shear stress (τ_{peak}), initial normal stress ($\sigma_{n,i}$). $U1$ is the shear displacement at the point where peak shear stress was reached.

3.5.1 Elastic CND with scaled joint surface

In an attempt to observe the effect of scaling, the CND model was run with both the top and bottom part scaled up horizontally by 100% so that the joint length is 200mm (Figure 3.19). Scaling was performed according to Figure 2.13 (a), where the joint surface is duplicated without increasing the size of the joint asperities.

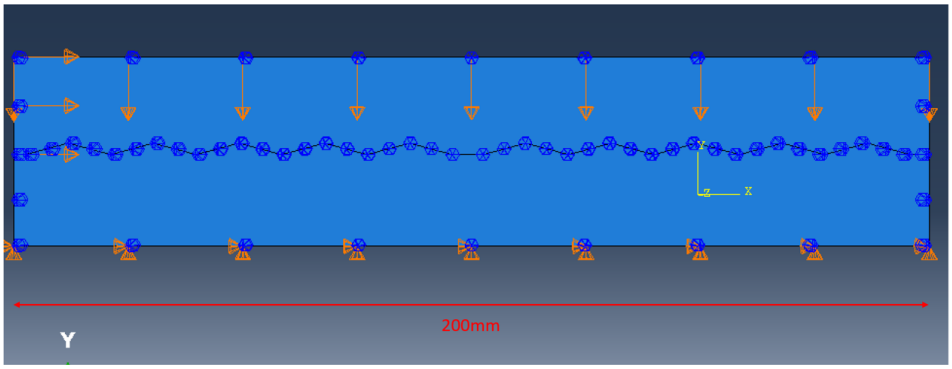

Figure 3.19: BC setup for 15.degree CND model with joint length scaled up to 200mm

The normal displacement in step-1 is set to 0.05 mm, the same as in the un-scaled model. When extracting the RFs for normal forces, normal stress was registered to be 7.13 MPa. For comparison, a normal load model was run with normal pressure set to 5 MPa. The registered result was 0.0478 mm.

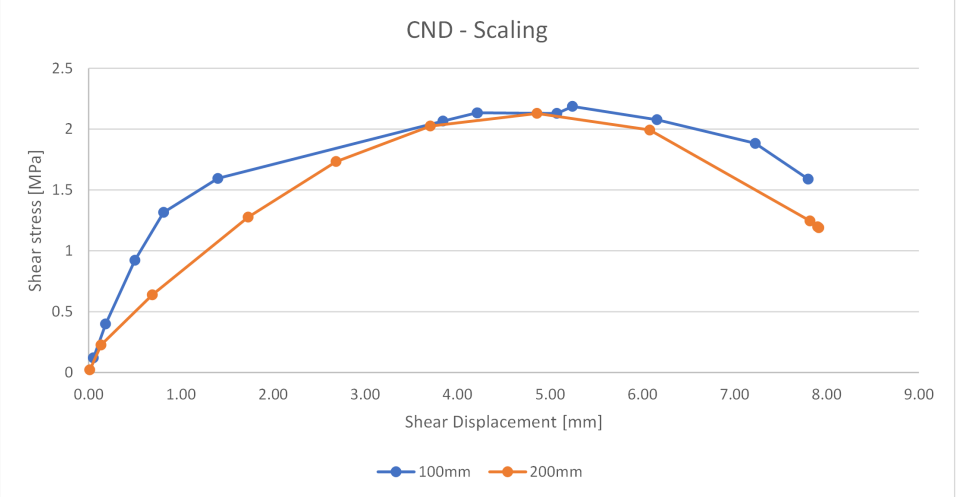

Figure 3.20: Stress-displacement plot for Elastic CND model with scaled joint length

Peak shear stress for the scaled model was measured at 2.12, which was marginally higher

than for the 100mm joint length model. The stress increase is also steeper for the scaled model, which is further elaborated in the section 4.2.

3.5.2 Elastic CND at different Young's modulus

Among the tests done on elastic models, the most prominent results compared to physical shear tests for rock samples were the elastic CND models for 15-degree saw-tooth asperities. In order to further evaluate models under these circumstances, these were again tested with tweaked input to observe the affected results when changing them. The following parameters were tested with the current CND model setup:

- E-modulus
- Poisson's ratio
- Quad and triangular mesh

Simulations were performed for E-modulus set to 2000, 4200, and 6000 MPa. Since it's preferred to have normal displacement set to 0.05 mm, which equals 5 MPa for the 4200 model, in order to compare the effect of this particular parameter, a load model has to run each time a material parameter is changed.

Table 3.5: Shear-displacement results at different Young's Modulus (E)

Input			**Output**	
E [MPa]	U_n [mm]	ν	P_i [MPa]	τ_{peak} [MPa]
2000	0.05	0.3	2.42	0.87
4200	0.05	0.3	5.01	1.82
6000	0.05	0.3	7.26	2.6

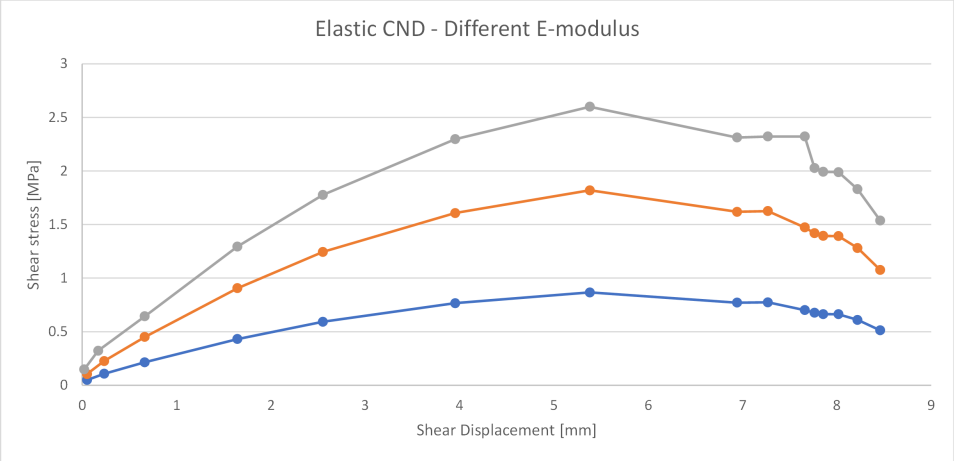

Figure 3.21: Shear stress-displacement for CND model using different Young's modulus

Table 3.5 and Figure 3.21 show simulation results for different E-modulus. Predictably,

the peak shear stress and shear stiffness of the model increased with an increased E-modulus.

3.5.3 Elastic CND at different Poisson's ratio

Similar to the E-modulus, the CND model is run using different Poisson's ratio, set to 0.2, 0.3, and 0.4.

Table 3.6: Shear-displacement results at different Poisson's ratio (ν)

Input		**Output**		
ν	U_n [mm]	P_i [MPa]	τ_{peak} [MPa]	U1 at peak [mm]
0.2	0.05	4.99	1.73	6.06
0.3	0.05	5.08	1.82	5.38
0.4	0.05	5.19	1.84	6.32

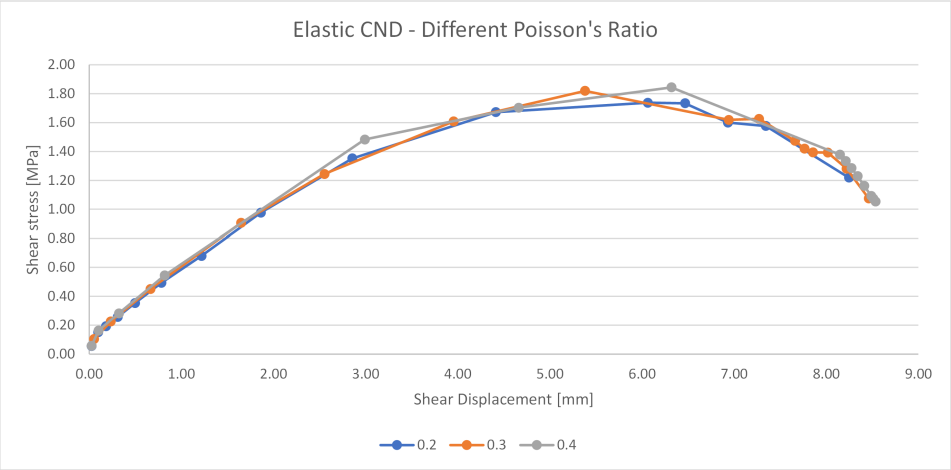

Figure 3.22: Shear stress-displacement for CND model using different Poisson's ratio

Results shown in Table 3.6 and Figure 3.22 show a slight increase in peak shear stress with increased Poisson's ratio. This is most apparent from 0.2 to 0.4 as the sampled increments lie very close to each other. Variations between 0.3 and 0.4 may be mainly due to uneven sampling.

3.5.4 Elastic CND with different mesh geometry

In all models prior, only quad mesh was used. While keeping all other parameters the same, simulations were run after changing mesh element types from quad- to tri-elements. Tri-mesh elements have been used in other modeling work for rock mechanics, for example, JianPing et al. 2015. Figure 3.23 shows the mesh for both models. In both cases, "Approximate global size" was kept at 1 for global seeds, so one element remained the equivalent of 1 mm.

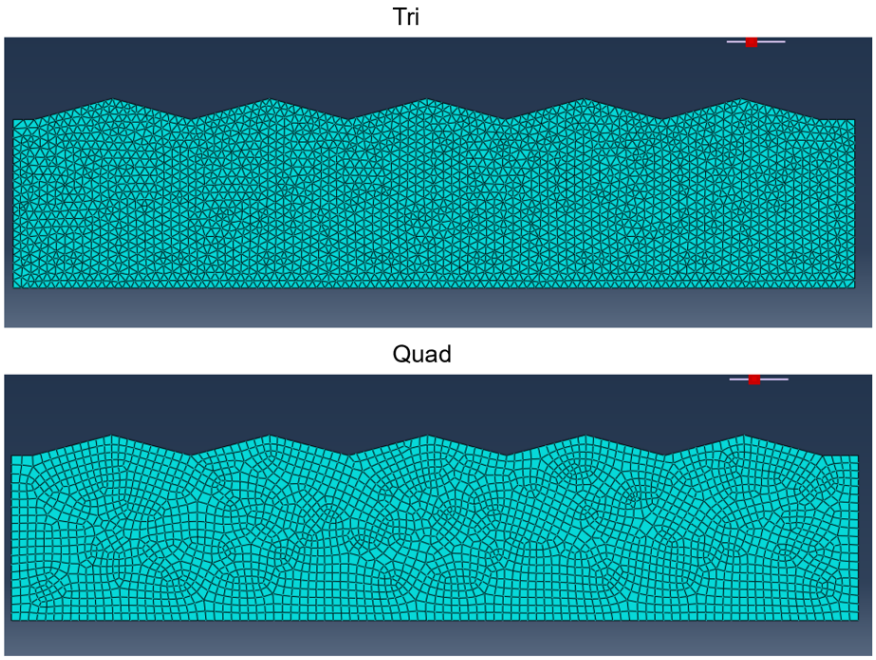

Figure 3.23: Bottom part of the saw-tooth model with quad- and tri-mesh elements

Figure 3.24 and Table 3.5 show simulation results for the two models. Interestingly, the tri-mesh simulation had a slightly higher peak shear stress than the quad-mesh model. Both models aborted at the same horizontal displacement.

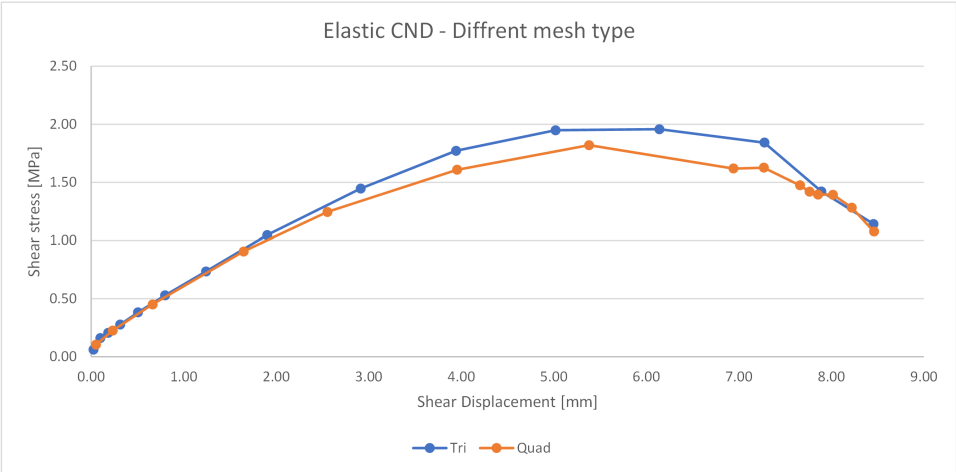

Figure 3.24: Shear stress-displacement for CND model using different mesh types

Table 3.7: Shear-displacement results with different mesh types

Input	**Output**		
U_n (mm)	P_i (MPa)	τ_{peak} (MPa)	U1 at peak (mm)
Tri	5.11	1.96	6.14
Quad	5.08	1.82	5.38

From the output for P_i, the quad-mesh resulted in a value closer to the analytical value for solid rock and was therefore used for the remaining models, as no factors suggested doing otherwise.

3.6 Elastic CNL models - shear under normal load

For this section, the CND model is copied and normal- and shear displacement is replaced with normal and shear load in steps 1 and 2 (Figure 3.25). Similar conditions to the 0.5 mm normal displacement model are compared to this one, where the normal load is set to 5MPa and the shear load is set to 1, 2, 5, 8, 10, and 20 MPa for comparison. A key difference between CNL and CND models is that vertical displacement may occur in the CNL model. For that reason, change in vertical displacement is monitored for the different shear loads.

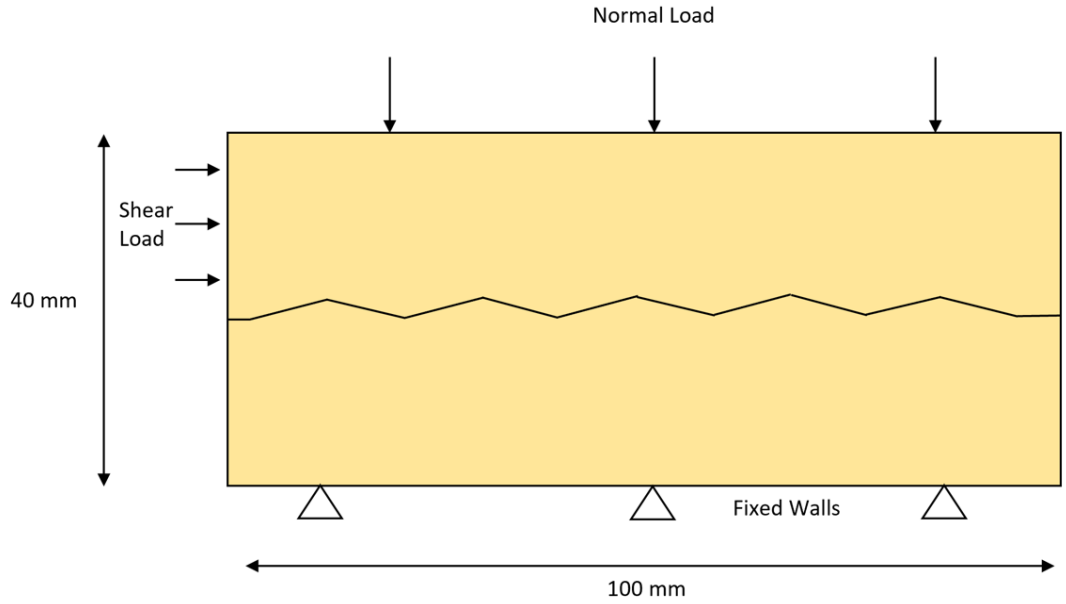

Figure 3.25: Concept illustration of CNL model

A regression model is also run for CNL to find the comparison between the shear load initiated and the shear load registered through RFs (Table 3.8). This model is also used to identify some trends that separate it from the CND model. The time period for each step is initially set to 10 seconds. The effect of time increment is discussed in section 3.6.1.

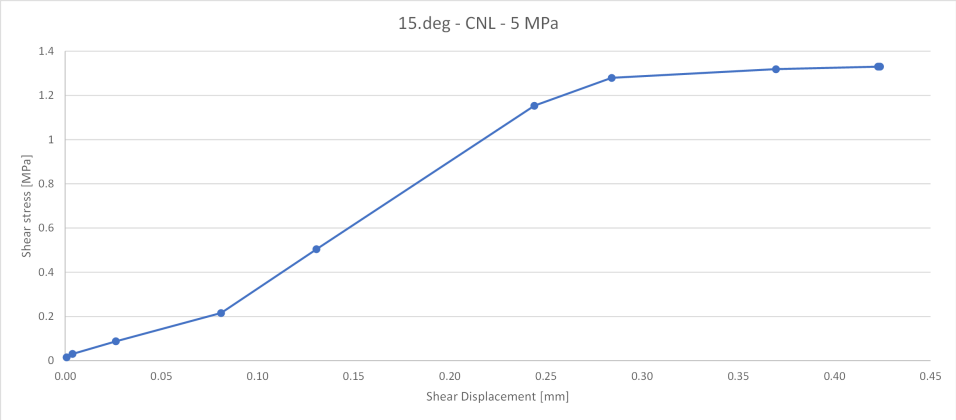

Figure 3.26: Shear stress-displacement for CNL to last converged increment

As it was clear that the shear stress registered was different for the different levels of applied shear pressure, this aspect of the CNL model was further reviewed. For the CND models, a horizontal displacement would be run until the model is aborted. At that point, the shear stress would already be trending downward. For the CNL models, however, shear stress was still trending upward as the model was aborted. The CNL model was therefore run at different applied shear stresses to monitor the effect of this input. Stress and displacement results for these models are shown in Table 3.8 and Figure 3.27.

Table 3.8: Elastic CNL results

P_s [MPa]	σ_s [MPa]	$\Delta U1$ [mm]	$\Delta U2$ [mm]	$\Delta\sigma_n$ [MPa]	σ_s/P_s
1.0	0.2676	0.0083	0.0003	0	26.8
3.0	0.5700	0.0302	0.0012	0	19.0
5.0	0.9500	0.0558	0.0025	0	19.0
6.0	1.1400	0.0786	0.0051	0	19.0
8.0	1.3303	0.4235	0.0849	0	16.6
10.0	1.3430	0.4237	0.0849	0	13.4
20.0	1.3430	0.4276	0.0857	0	6.7

Both 10 MPa and 20 MPa models were run until the last converged increment and achieved the same results in stress and displacement. For all models that converged, outside of the lowest shear pressure of 1 MPa, the registered initial shear stress from RFs, was approximately calculated to 19% of the shear load input when using the same calculation method as for normal load.

For insurance, this was tested for a single block 1-part model, where the sum of forces was found to be similar. Since the area of the applied force was 1/5 of the top surface, these results are logical. As the shear stress is given by the sum of reaction forces divided by the area of the applied pressure, this was adjusted for.

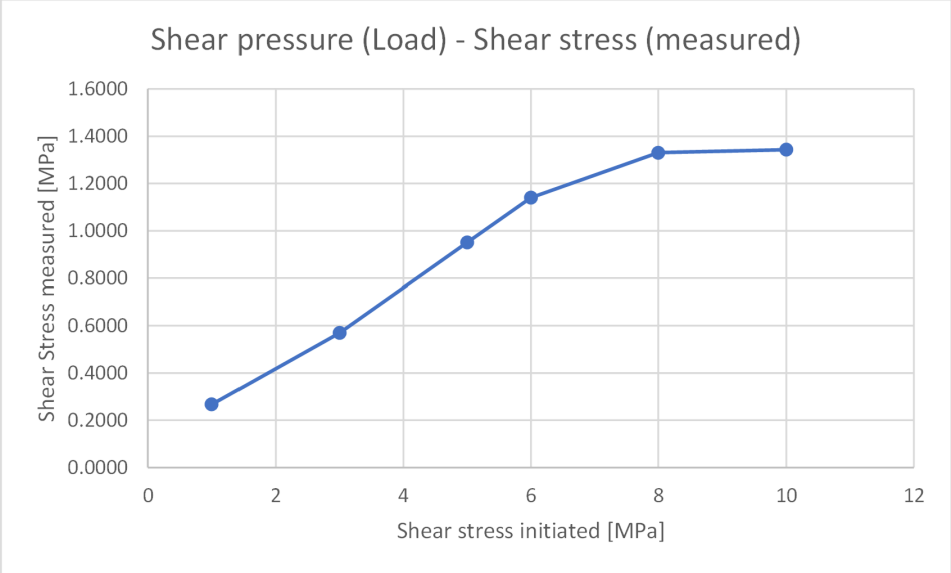

Figure 3.27: Vertical displacement for CNL at 1 MPa normal load. Non-uniformly distributed normal displacement

The concluded use of shear pressure input was using a pressure higher than normal pressure (adjusted for the pressure area between the top and the side of the block).

3.6.1 Use of time period in CNL

From a few simulations using different step periods. The shear displacement and stress measured through RFs were unchanged with the increased time period, attempting with values from 1 to 100 seconds. However, the peak stress and displacement values were close to identical regardless of the time period used. Figure 3.28 shows the result of simulations done with different time periods, all of them with increment size 0.01 and a maximum number of increments of 1000.

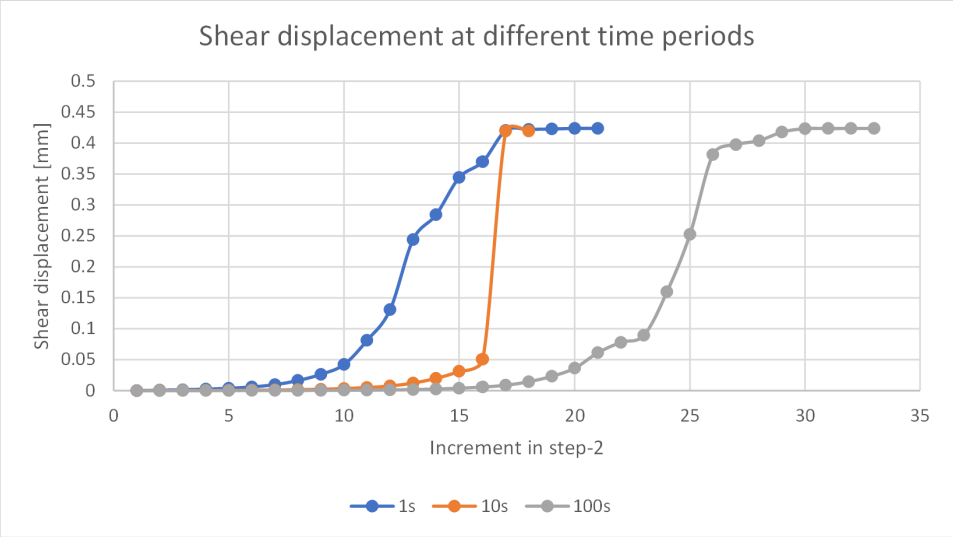

Figure 3.28: Shear displacement when defining the time periods of the shear step as 1, 10, and 100 seconds.

For elastic models, the main point of interest in this aspect is related to the stress displacement curves for CNL models. With the longer time periods used, more plot points are lost and leave incomplete data sets for comparison. In addition to this, using the method of manually extracting data for each plot point makes for a much simpler task in choosing data points that give a good representation of stress-displacement curves.

Aborted models occur when initiated shear load exceeds the normal pressure. In these cases, the normal displacement at the last converged increment is larger than the initial displacement at zero when using frictionless contact parameters. Figure 3.29 show the history output for U2 when using constraints along the top surface and does not account for the distribution of displacement.

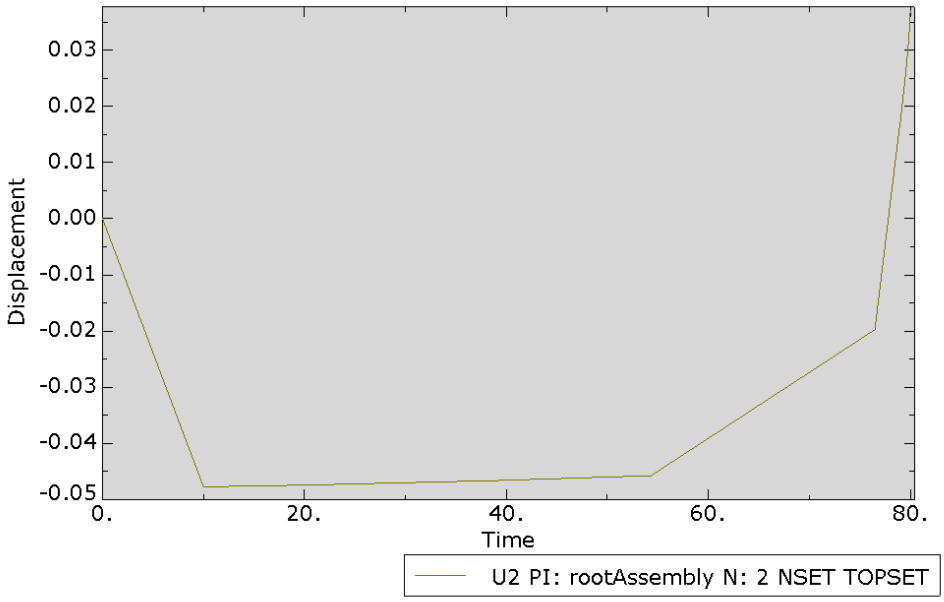

Figure 3.29: Normal displacement during shear load of frictionless CNL model

As Figure 3.30 shows the last converged increment for a CNL model, Figure 3.31 shows the dynamics of the top block moves in y-direction throughout the simulation with zero normal displacements being before the initial normal load. With that, the starting point in the plot is after the 5 MPa normal load is set.

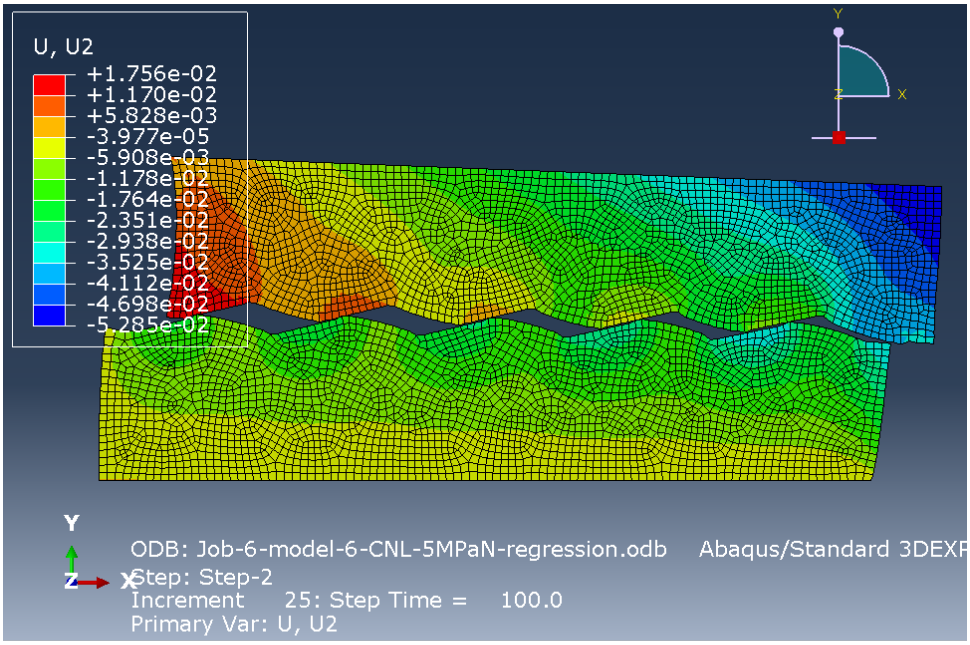

Figure 3.30: Shear stress-displacement for CNL to last converged increment

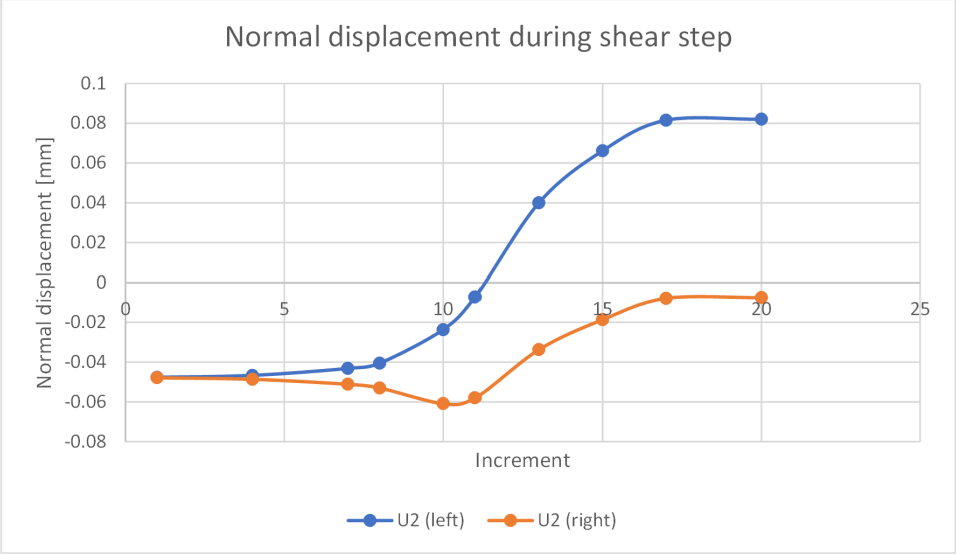

Figure 3.31: Normal displacement for the left and right side of the top block during a CNL shear test

Predictably, the left side of the block raised higher than the right side. However, at the point where the left side starts to increase, the right side is pushed further down from the initial normal displacement. As the last increment is reached, the curves have flattened

out. This is at the point where the stress-displacement curve for the same simulation (Figure 3.26) has reached its peak.

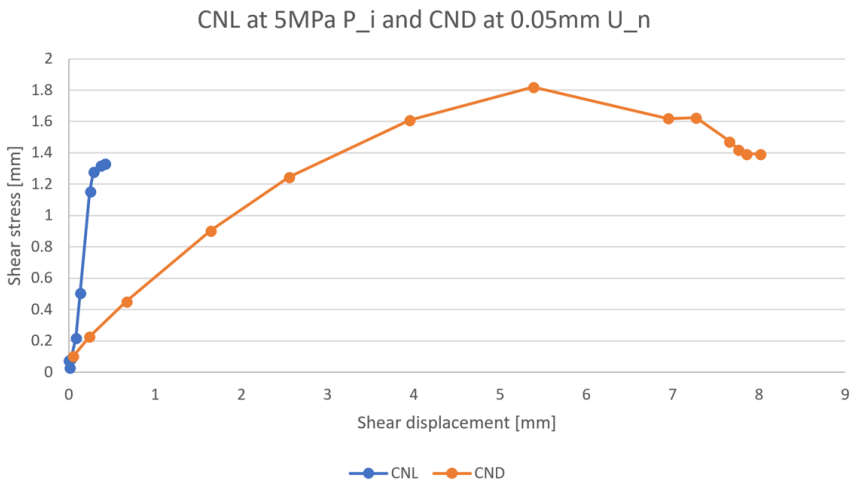

Figure 3.32: Shear stress-displacement plot for CND at 0.05mm normal displacement and CNL at 5 MPa normal pressure

Putting the CND and CNL models in the same plot is shown in Figure 3.32, both using 15. degree saw-tooth asperities and the same material parameters. First, the CNL model aborts before the plot starts trending down, at which point it's unclear whether a peak is reached. This also occurs at a much smaller displacement than for the CND model. These are expected results when compared to numerical studies in the literature.

3.7 Plastic 2D CNL model

With established models for elastic behavior, the next step included adding plastic material parameters. Assuming the behavior shown in Figure 2.8, shearing occurs when the shear stress-displacement approaches peak shear strength. With added plastic parameters, this should, in theory, have a more realistic simulation of rock mass, especially ductile rock types.

The minimum requirement for material parameters in ABAQUS when using M-C plasticity is Young's Modulus, Poisson's Ratio, friction angle, dilation angle, and cohesion yield stress. It's also possible to add tension cut-off. In the context of verification through lab tests found in literature, acquiring all these parameters poses a challenge. When shearing reaches the point where asperity crushing is realistic, generating fractures requires additional damage parameters, which again are difficult to acquire. As discussed in an earlier section, some more widely used experimental data from literature used for numerical verification include (S.C Bandis et al. 1983, Barton and Choubey 1977 and Patton 1966). While all of them contain relevant laboratory test results on a varied selection of rock samples, neither contains all data needed for input in the ABAQUS model for fracture simulation.

In simulation prior to this section, results have been closely compared to Bahaaddini et al. 2013. For this section, it's possible to compare areas of plastic deformation to where fractures occur along the asperities in the PFC2D models. No experimental study found describes where fractures occur in this type of shear test.

For a more realistic shear test simulation, it's possible to add parameters in material properties. This was unsuccessfully attempted with multiple of the damage-material options available in ABAQUS. Even with a converged model with these options, no material data for any of those criteria were found.

Table 3.9: Input for Plastic 2D CNL model

Material parameters	
Density	2.6 x 10^{-9} tonne/mm3
Young's Modulus	4200 MPa
Poisson's ratio	0.3
Friction Angle	30
Dilation angle	1 (assumed)
Cohesion Yield stress	15
Tension Cutoff	10
Interaction parameters	
Friction Coefficient	0.05
Load (CNL)	
Normal	5 MPa
Shear	8 MPa
Displacement (CND)	
Normal	0.05 mm
Shear	10 mm

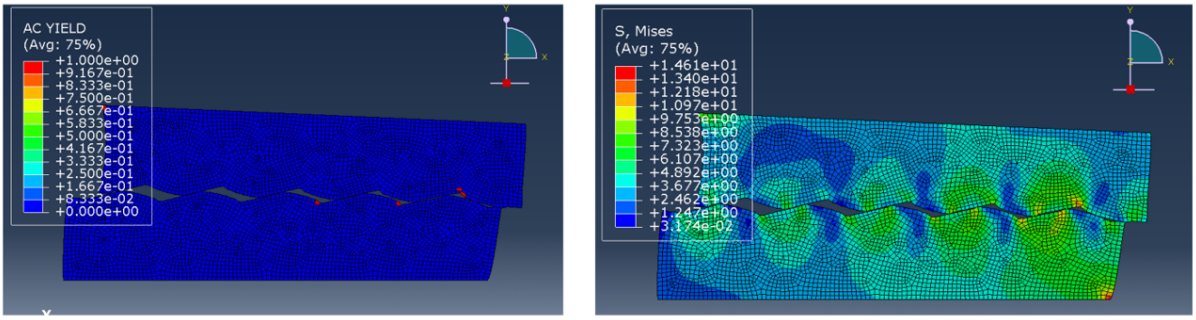

Figure 3.33: Stress (left) and AC Yield (right) of plastic CNL simulation

From the side-by-side plot in Figure 3.34, it is shown that for the CNL simulation, added plastic material parameter had approximately no effect on the stress-displacement development during the shear process. It's also clear that at the last converged increment, the shear stress was still trending upwards, making it unclear whether the true peak displacement was reached.

From Figure 3.33, it's shown that some plastic deformation did occur to a small extent. Even if this had no effect on peak shear stress, the area of plastic deformations did resemble the areas from where fractures occurred in the compared PCF2D models for saw-tooth asperities of the same dilation angle (Bahaaddini et al. 2013). The compared

models are shown in Figure 2.12, where fractures first occur in the "valley" parts of the asperities where they are the widest.

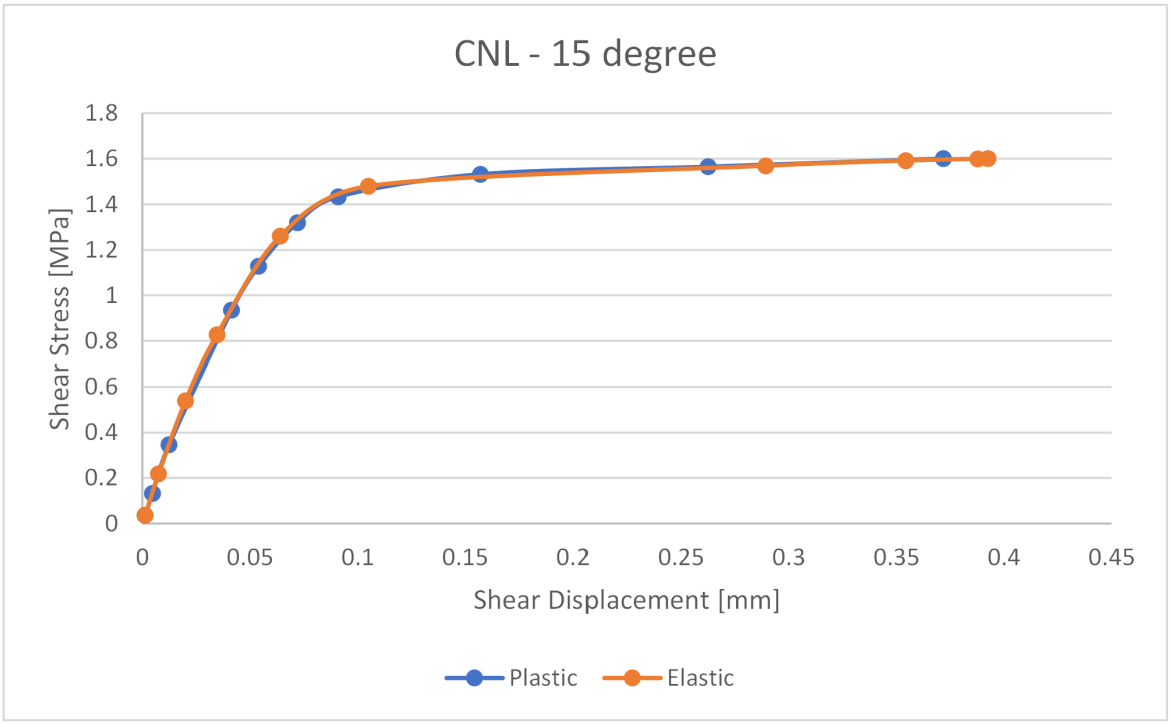

Figure 3.34: Stress-displacement plot of 15.degree CNL model with and without added plastic parameters (M-C)

The first plastic CNL model showed similar results to the elastic model. Figure 3.34 indicates where Yielded elements occur, as well as the stress mises for the same increment.

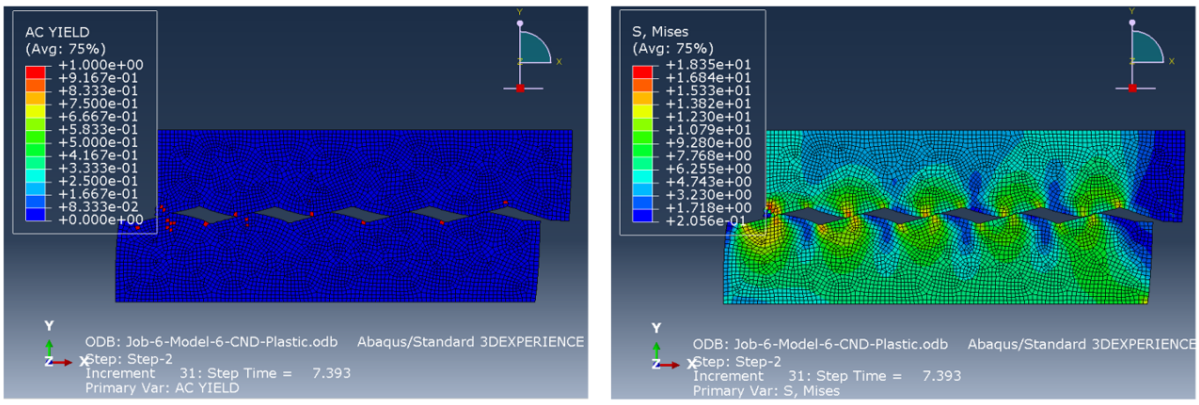

Figure 3.35: Stress (left) and AC Yield (right) of plastic CND simulation

Compared to the CNL model, the plastic CND resulted in more yielded elements, still close to the triangular asperities. However, in the CND case, the plastic deformation is more apparent on the left side of the sample, where the highest stress levels are located. When attempting to reduce tension cut-off.

The first attempt at a shear model with plastic deformation criteria was able to generate yielded elements distributed at areas that are similar to fractures that were simulated in Bahaaddini et al. 2013, (Figure 2.12). In both cases, the majority of fractures occurred along the tips and center of the asperities.

3.8 35.degree plastic CND model

As other numerical studies had attempted the same, saw-tooth models with larger asperity angles were simulated with plastic material properties. In Bahaaddini et al. 2013, the 35.degree asperity angle model resulted in the most fractures, giving the idea that with added plasticity to the elastic CND model, stress-displacement results would, to a larger degree, be affected by the plasticity. The setup for the 35.degree model is shown in Figure 3.36.

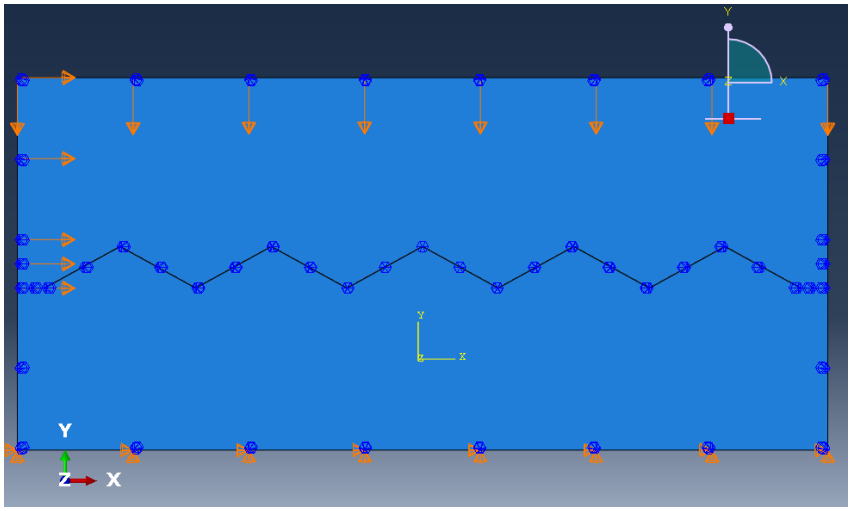

Figure 3.36: BC setup for 35.degree asperity plastic model

From the simulation results, yielded elements were, to a large degree, focused on the left-side asperity closest to the initiated displacement boundary conditions. From PCF2D results in Figure 2.12, fractures did occur at a similar angle as yielded elements in this model for some of the central asperities. As the stress patterns for this fracture model more closely resembled the CNL conditions, it's possible that CNL models would more accurately replicate this fracture pattern. Unfortunately, the 35.degree CNL model was unable to converge at a stage where yielded elements gave any good results.

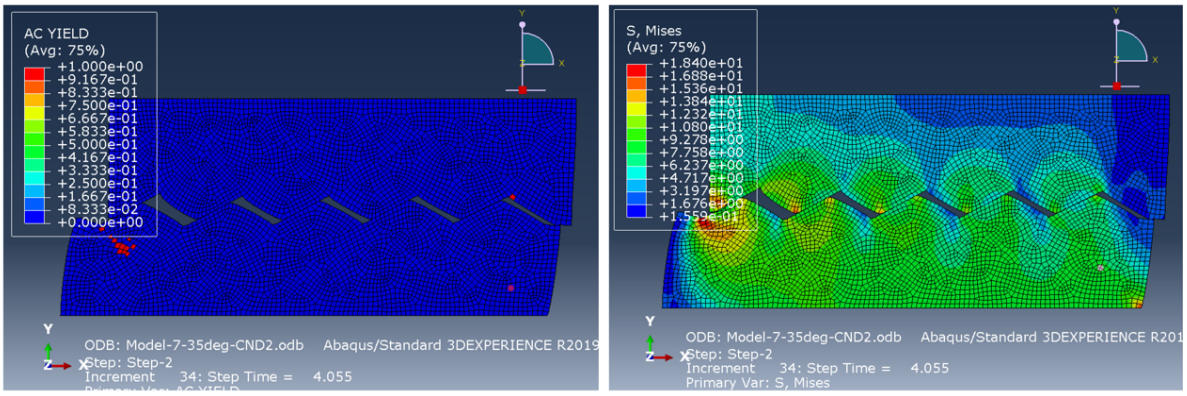

Figure 3.37: Stress result and yielded elements for 35.degree asperity plastic model

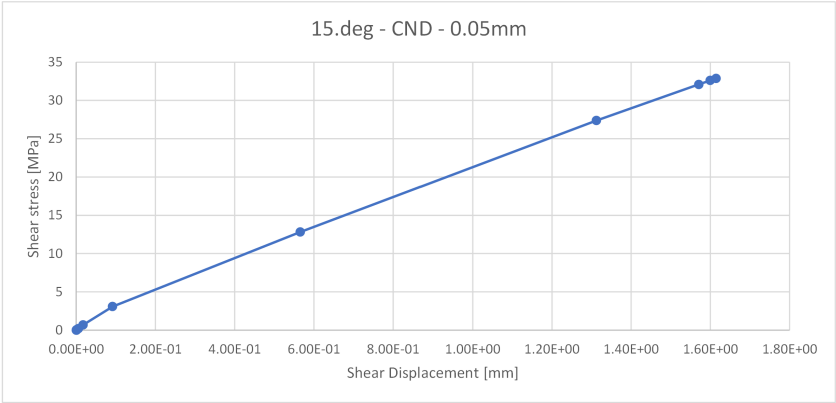

Figure 3.38: Stress-displacement plot for 35.degree asperity plastic model

From the stress-displacement plot in Figure 3.38, linear relation continued to the last converged increment. This continued to shear stress at 33 MPa, making it clear that the results were highly unreliable.

4 Discussion

4.1 Evaluation of model aspects

In the process of creating a numerical simulation of direct shear tests, all requirements for a standard FEM model were experimented with in order to find what changes would result in the converged model that came closest to replicating an actual laboratory experiment. Optional model inputs, such as frictional properties, damage parameters, etc., were attempted to implement with varying results.

The following section explains the most important takeaways from the trial and error process of the modeling work in the case that this was to be used in future work.

4.1.1 Parts

Of the different part geometries that were used, the one that came closest to giving realistic shear test results was the 15-degree interlocked saw-tooth model with elastic material parameters. All parts used were at 100x20 mm with some variance due to asperities. Using mismatched geometries would always result in the model aborting before a shear step could be introduced. The sensitivity study experimented with using different uneven surfaces. This included geometries such as rounded asperities and evenly distributed saw-tooth asperities. Only the interactions that did not include any type of "sharp edges" ended up aborting at a maximum of three contact points reached.

For the successful interlocked saw-tooth models, it was the "sharp asperity tips" that caused convergence issues for mismatched surfaces that were able to reach 318 MPa normal stress when normal displacement was 3.12 mm, with the dimensions used for the parts.

All shear models tried for 35.degree dilation asperities; shear behavior was measured to unrealistically high shear stress levels.

4.1.2 Mesh

For the mesh, a few different aspects were studied for the CND elastic 15. degree model, including:

- Mesh type: In-plane strain and in-plane stress
- Element geometry: Tri- and quad-elements
- Mesh density

The early choice of using plain strain was initially to be able to add plastic parameters for the 2D model while also eliminating mesh type as a source of error when comparing the model with the added plasticity. When comparing the elastic model after changing the mesh type from plane stress to plain strain, the results were identical.

Tri- and quad-elements were experimented with as these have both been used in similar studies. Both element types were able to converge at a similar rate. However, in the

shear stress-displacement plot for the two models, which shared similar development to about 50% of τ_{peak}, max shear stress τ_{peak} was marginally lower for the tri-mesh than for the quad-mesh. For the two simulations, the peak shear stresses reached 1.82 MPa and 1.96 MPa, respectively (Figure 3.23).

Mesh density had no effect on either convergence rate or stress-displacement results. Using finer mesh density did, however, prove to be helpful when using history output to analyze the distribution of the reaction forces along the bottom path (Figure 3.4). Especially for the normal forces, the distribution of the path had one spike of force about 1 mm from each of the sample walls, which could be a potential source of error. However, the sum of forces would be unchanged when using a finer mesh.

4.1.3 Interaction properties

Throughout most of the model work phase, interaction properties were kept at "Frictionless" for tangential behavior and "Hard contact" for normal behavior. For tangential behavior, it was experimented with using "Rough" and "Penalty" friction formulations. The "Rough" parameter works so that "No slips will occur once points are in contact". As the joint surfaces are 100% in contact from the initial stage, the model would behave like a solid block, where the two parts were merged without any joint between them. Penalty would allow a friction coefficient to be defined. This would result in the CNL models aborting at an earlier stage.

The choice between using the top or bottom surface as slave- and master surface would have no effect on the results.

4.1.4 Material Parameters

When using basic elastic properties and M-C plasticity, no model issue would occur relating to material parameters. As a realistic shear test would involve eventual fracture damage to the material, several mechanical damage parameters were experimented with, including "Shear damage", "Ductile damage", and "Johnson-Cook damage". Each of these would result in the model being unable to run.

For the plastic models, despite the fact that there were no changes between the elastic model when adding M-C Plasticity, some yielded elements would be found in post-processing. The yielded area would increase when reducing "tension cut-off" in material parameters, indicating tension deformation in the material. The area for yielded elements would also correspond with where fractures were found in Bahaaddini et al. 2013 (Figure 2.12).

4.1.5 Boundary conditions

Due to the varying circumstances for direct shear testing, a number of different uses of boundary conditions were tested. These changes usually concerned the 0-displacement in the x-direction for the top and bottom block, as well as how close to the asperities the displacement or 0-displacement would change.

Overcomplicating the changing of BCs between the steps only resulted in creating more problems than it solved, as more added steps would make the post-processing phase troublesome while also having little to no effect on stress-displacement development. The most successful BC setup ended up only having the bottom surface pinned and the remaining boundaries only having 0-displacement in the z-direction. The only change between step-1 and 2 is the added vertical step for load or displacement, depending on which CNL or CND model is being used.

To address the problem of achieving desired normal load for the CND model, the best way used was to run a model with the pressure load first, registering the normal displacement in post-processing, and using the results as the normal displacement for the CND model.

4.1.6 Post-processing

A common approach when acquiring results in ABAQUS is defining history output requests for the desired data. For this study, that worked only for the displacement in the CNL models. When trying this method for reaction forces, no values would be registered for any of the surfaces. The only method that proved successful for acquiring reaction forces was defining a path in post-processing. This method was also useful for finding displacement for the CND models, where history output did not work. This made it possible to create stress-displacement plots by saving XY-data for a sufficient number of increments for both reaction forces and top block displacement.

This was, however, a cumbersome method, which would take a few minutes after each simulation before it could be possible to view the plot. This method also won't guarantee finding the true peak shear stress as it might not be included in the increments used. This could be caused either by defined incrementation in pre-processing or by the random selection of increments in post-processing.

Being able to register reaction forces in post-processing from history output, this problem has the potential to become a lot simpler. By then defining a more frequent incrementation in pre-processing, it's possible to create much more accurate stress-displacement plots without using excessive amounts of time. ABAQUS also has the option to access history output through Python script, which again has the potential to simplify this task. With having to use paths in post-processing, it was not possible to do this.

4.2 Evaluation of simulated joint behavior

Despite the simplifications done for the numerical models compared to lab research of actual rock samples, some of the stiffness calculation methods were implemented for the stress-displacement plots of the numerical models. Peak shear stress is assumed to be the highest sampled shear stress, including for the models that did not result in a complete curve. Shear stiffness methods used include the traditional linear shear stiffness (equation 2.6) for both secant- and tangent methods. Barton-Bandis stiffness (equation 2.9) Requires the parameters JRC and JCS, which are not implemented in the model. For simplicity's sake, JRC can be estimated based on the dilation angle and JCS based

on E-modulus (equation 2.3). Note that this estimation was performed for samples with relatively high values of E-modulus, comes with a large standard deviation, and is, in this case, used as a placeholder for actual mechanical properties.

Since E-modulus used for all models included in this section are at 4.2 GPa, JCS will be estimated with equation 2.4 (Malik et al. 1997):

$$JCS[MPa] = 0.0084 \times E[MPa]$$

$$JCS[MPa] = 0.0084 \times 4200 = 35.3MPa$$

With these assumptions:

$$k_s = \frac{100}{L} \cdot \sigma_n tan[JRC\, log_{10}(\frac{JCS}{\sigma_n} + \phi_r)]$$

$$k_s = \frac{100}{100} \cdot \sigma_n tan[15\, log_{10}(\frac{35.3\, MPa}{\sigma_n} + 30)]$$

ϕ_r showed that plastic parameters had little to no effect on the shear stress-displacement curve. As $\phi_r = 30$ was used for the plastic model, it's included here as well. Table 4.2 and 4.1 shows the results of shear stiffness for the different normal displacements. The stiffness calculation methods are explained as follows:

- secant (peak)-method: Linear from lowest to highest stress value (Figure 4.1)
- Tangent-method: Linear tangent set at 50% of peak shear stress (Figure 4.1)
- Barton-Bandis (equation 2.9): Assuming JRC being dilation angle (ı) and JCS estimated from equation (2.4)

Table 4.1: Linear secant shear stiffness measured for elastic CND models with 15.degree triangular asperities at different normal displacement

U_n [mm]	τ_{peak}	$\sigma_{s,60}$ [MPa]	$\sigma_{s,40}$ [MPa]	$U1_{60}$ [mm]	$U1_{60}$ [mm]	k_s [MPa/mm]
0.01	1.77	1.062	0.708	2.27	1.41	0.41
0.02	1.88	1.128	0.752	1.71	0.70	0.36
0.03	2.01	1.206	0.804	1.34	0.64	0.52
0.05	2.18	1.308	0.872	1.68	0.87	0.36

Table 4.2: Linear secant shear stiffness measured for elastic CND models with 15.degree triangular asperities at different normal displacement

U_n [mm]	τ_{peak} [MPa]	τ_{min} [MPa]	U1 at peak [mm]	U1 at min [mm]	k_s [MPa/mm]
0.01	1.77	0.067	5.40	0.084	0.32
0.02	1.88	0.141	5.79	0.061	0.30
0.03	2.01	0.121	4.35	0.050	0.44
0.05	2.18	0.120	5.24	0.052	0.48

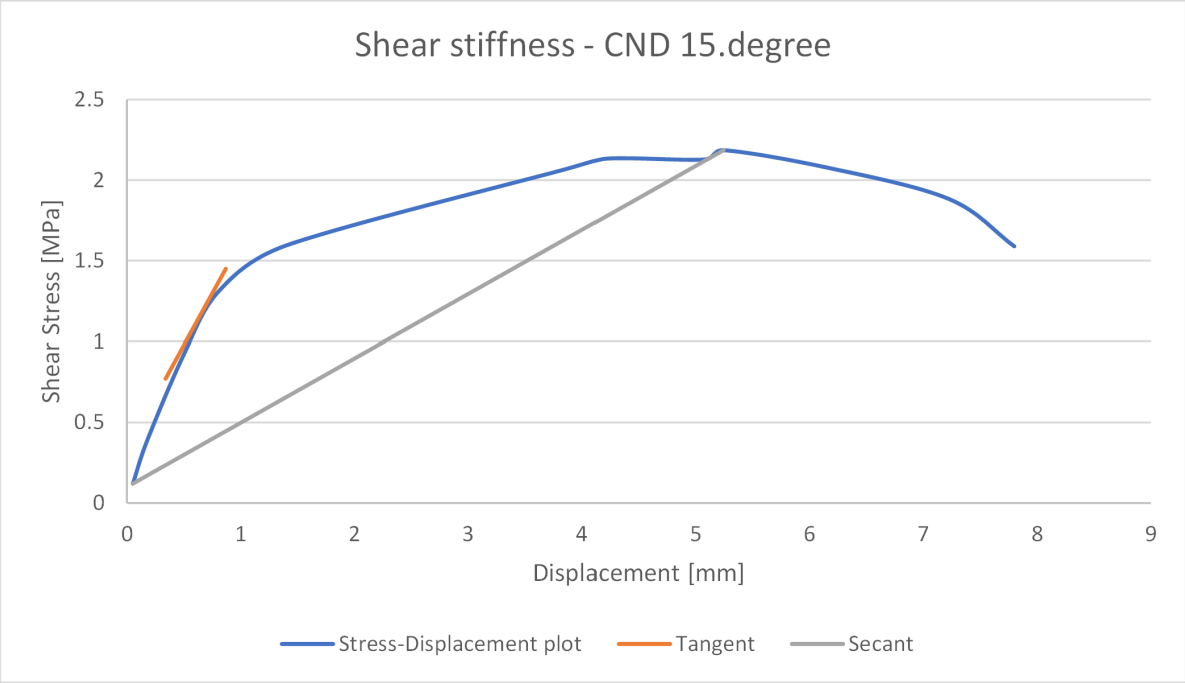

Figure 4.1: Linear stiffness (tangent and secant) for elastic CND model

Table 4.3: stiffness results for elastic CND models at different normal displacement (Figure 3.18)

U_n [mm]	σ_n [MPa]	k_s
0.01	1.016	0.521
0.02	2.032	0.953
0.03	3.047	1.375
0.05	5.079	2.210

Upon viewing the shear stiffness results from the Barton-Bandis method, it's clear that they drastically overestimate the shear stiffness compared to the two linear methods. The Barton-Bandis method assumes constant normal stress, which the simulation results for CNL models indicate, should also have a higher shear stiffness as it reaches its peak at

a much lower displacement (Figure 3.32). For that reason, the same three methods were used for the elastic CNL model (Figure 3.17). Stiffness results for the CNL model are shown in Table 4.4.

Table 4.4: Shear stiffness for some of the models using different stiffness criteria (all values in [MPa/mm])

	Secant	Tangent	Barton-Bandis
CND 15 deg elastic (Figure 3.20)	0.48	1.26	2.210
CNL 15 deg elastic (Figure 3.26)	3.13	5.90	2.217
200mm scaled elastic (Figure 3.20)	0.61	0.43	1.015

From the results in Table 4.4, some things are worth pointing out. First, Barton-Bandis shear stiffness for the scaled CND joint will be reduced by 50% when the joint length is doubled. Note that this scaling utilizes the scaling method in (a) of Figure 2.9. This reduced stiffness with scaling was also indicated by the stress-displacement comparison between the scaled and the unscaled CND model (Figure 3.19),

Second, CNL stiffness calculation was highly unreliable for the same reason that the model itself was deemed unreliable. As the shear stress is still trending upwards at the last increment, the calculated stiffness would depend entirely on the "Plateau-length" of the plot. As shown in the plastic 35.degree model, this would approach an extremely high value.

5 Conclusion

In the process of researching the behavior of rock mass, several numerical models were developed for simulating the shear process of a rough joint under different stress conditions. The joint roughness was represented through triangular saw-tooth joints at different dilation angles, inspired by other experimental and numerical research done in the past. As multiple variations of these models were tested, the simulations that came closest to realistic shear behavior were the models which contained the following factors:

- Constant normal displacement
- 15.degree roughness
- 100% contact area between the two joint surfaces
- Quad-dominated mesh geometry
- No plastic parameters
- Frictionless surface interaction

The models with this description were able to recreate a number of well-known phenomena in rock mechanics. Which includes:

- Realistic peak shear stress for rough joint surfaces, ranging between 1 MPa - 3 MPa for rough joint surfaces with small levels of normal stress.
- Increased peak shear stress for higher normal stress/displacement during shear movement
- Decreased shear stiffness for rough joints when the joint length is scaled up
- Increased shear stiffness and peak shear stress when increasing E-modulus

A few of the attempted models were concluded as unsuccessful in simulating realistic shear behavior. However, they did show some promising signs which could be worked upon further. These include:

1. Normal closure of mismatched joints created hyperbolic stress-displacement curve as contact points between the surfaces increase
2. Elastic CNL models followed at realistic shear stress-displacement development to a peak stress range that was comparable to experimental research
3. CND and CNL models with added plastic parameters (Mohr-coulomb plasticity with tension cut-off) were able to simulate yielded elements in areas that were in agreement with similar studies on shear tests on saw-tooth joints

Item 1 had the issue that the model would crash when only three contact points had occurred between the surfaces, at which point normal stress and displacement were nowhere near the peak. Because of this, an added shear step was impossible. Pinpointing the reason for convergence error at this stage could open up the opportunity to improve on the working shear models. For item 2, it's necessary to find a clear way to determine

peak shear stress. Experimental research suggests that the addition of realistic fracture simulations would be able to help in this area, as asperities crushing will need to occur for the downward stress-displacement trend. Item 3 would also benefit from the addition of fracture simulation.

Another point of improvement would be a more convenient method of extracting test results, as history output defined in pre-processing was unable to register reaction forces automatically. Automating this process would heavily reduce the work of exporting and analyzing simulation results. This would also make it possibly easier to utilize more plot points for the deformation curves and, by that, avoid errors related to the frequency of plot points.

References

ABAQUS-Manual, Dassaul Syst (2014). *GETTING STARTED WITH ABAQUS: INTERACTIVE EDITION*. English. Version 6.14. Thorlabs. 693 pp.

Bahaaddini, M, G Sharrock, and BK Hebblewhite (2013). "Numerical direct shear tests to model the shear behaviour of rock joints". In: *Computers and Geotechnics* 51, pp. 101–115.

Bandis, S.C, A.C Lumsden, and N Barton (1983). "Fundamentals of Rock Joint Deformation". In: *International journal of rock mechanics and mining sciences*, pp. 249–268.

Barton, N and S Bandis (1982). "Effects of block size on the shear behavior of jointed rock". In: *The 23rd US symposium on rock mechanics (USRMS)*. OnePetro.

Barton, N and V Choubey (1977). "The shear strength of rock joints in theory and practice". In: *Rock mechanics* 10, pp. 1–54.

Barton, N.R (2013). "Shear strength criteria for rock, rock joints, rockfill and rock masses: Problems and some solutions". In: *Journal of Rock Mechanics and Geotechnical Engineering* 5.4, pp. 249–261.

Castelli, M et al. (2001). "Experimental evaluation of scale effects on the mechanical behavior of rock joints". In: *Rock mechanics-A challenge for society*, pp. 205–212.

Fairhurst, C (1964). "On the validity of the 'Brazilian'test for brittle materials". In: *International Journal of Rock Mechanics and Mining Sciences & Geomechanics Abstracts*. Vol. 1. 4. Elsevier, pp. 535–546.

Giani, GP et al. (1995). "Scale effect evaluation on natural discontinuity shear strength". In: *Fractured and jointed rock masses*, pp. 447–452.

Goodman, R.E, R.L Taylor, and T.L Brekke (1968). "A model for the mechanics of jointed rock". In: *Journal of the soil mechanics and foundations division* 94.3, pp. 637–659.

Goodman, RE (1970). "The deformability of joints". In: *Determination of the in situ Modulus of Deformation of rock*. ASTM International.

– (1974). "The mechanical properties of joints". In: *Proc 3rd Int Congr International Society of Rock Mechanics*, pp. 1–7.

Hencher, SR, JP Toy, and AC Lumsden (2020). "Scale dependent shear strength of rock joints". In: *scale effects in rock masses 93*. CRC Press, pp. 233–240.

Hungr, O. and D.F Coates (1978). "Deformability of rock joints and its relation to rock foundation settlements". In: *Can. Geotech*, pp. 239–249.

JianPing, Yang et al. (2015). "Numerical determination of strength and deformability of fractured rock mass by FEM modeling". In: *Computers and Geotechnics* 64, pp. 20–31.

Kulatilake, Pinnaduwa HSW et al. (2016). "Laboratory estimation of rock joint stiffness and frictional parameters". In: *Geotechnical and Geological Engineering* 34.6, pp. 1723–1735.

Ladanyi, Bt and G Archambault (1969). "Simulation of shear behavior of a jointed rock mass". In: *The 11th US Symposium on Rock Mechanics (USRMS)*. OnePetro.

Lai, ZHF, KJ Douglas, and G Mostyn (2007). "The Strength of Rock Defects-Numerical Analysis of Scale Effects". In: *11th ISRM Congress*. OnePetro.

Lavrov, Alexandre (2017). "Fracture permeability under normal stress: a fully computational approach". In: *Journal of Petroleum Exploration and Production Technology* 7.1, pp. 181–194.

Liu, Xige, Wancheng Zhu, and Lankun Li (2020). "Numerical shear tests on the scale effect of rock joints under CNL and CND conditions". In: *Advances in Civil Engineering* 2020, pp. 1–15.

Locher, Hans Georg and Urs G Rieder (1970). "Shear tests on layered Jurassic limestone". In: *2nd ISRM Congress*. OnePetro.

Malik, MH and SAJID Rashid (1997). "Correlation of some engineering geological properties of the Murree formation at lower Topa (Murree district), Pakistan". In: *Geological Bulletin of University Peshawar* 30, pp. 69–81.

Packulak, Timothy RM et al. (2022). "New data processing protocols to isolate fracture deformations to measure normal and shear joint stiffness". In: *Rock Mechanics and Rock Engineering*, pp. 1–20.

Patton, Franklin Davis (1966). "Multiple modes of shear failure in rock". In: *1st ISRM Congress*. OnePetro.

Sachpazis, CI (1990). "Correlating Schmidt hardness with compressive strength and Young's modulus of carbonate rocks". In: *Bulletin of Engineering Geology and the Environment* 42.1, pp. 75–83.

Shrivastava, Amit Kumar and K Seshagiri Rao (2015). "Shear behaviour of rock joints under CNL and CNS boundary conditions". In: *Geotechnical and Geological Engineering* 33, pp. 1205–1220.

Snow, DT (1972). "Fundamentals and in situ determination of permeability". In: *Proc. ISRM Sympos., Stuttgart, Germany, Genl. Rpt. Theme* 1.6.

Ueng, Tzou-Shin, Yue-Jan Jou, and I-Hui Peng (2010). "Scale effect on shear strength of computer-aided-manufactured joints". In: *Journal of Geoengineering* 5.2, pp. 29–37.

Wang, Lichun and M Bayani Cardenas (2016). "Development of an empirical model relating permeability and specific stiffness for rough fractures from numerical deformation experiments". In: *Journal of Geophysical Research: Solid Earth* 121.7, pp. 4977–4989.

Wang, Yu and Adeyemi Emman Aladejare (2016). "Bayesian characterization of correlation between uniaxial compressive strength and Young's modulus of rock". In: *International Journal of Rock Mechanics and Mining Sciences* 85, pp. 10–19.

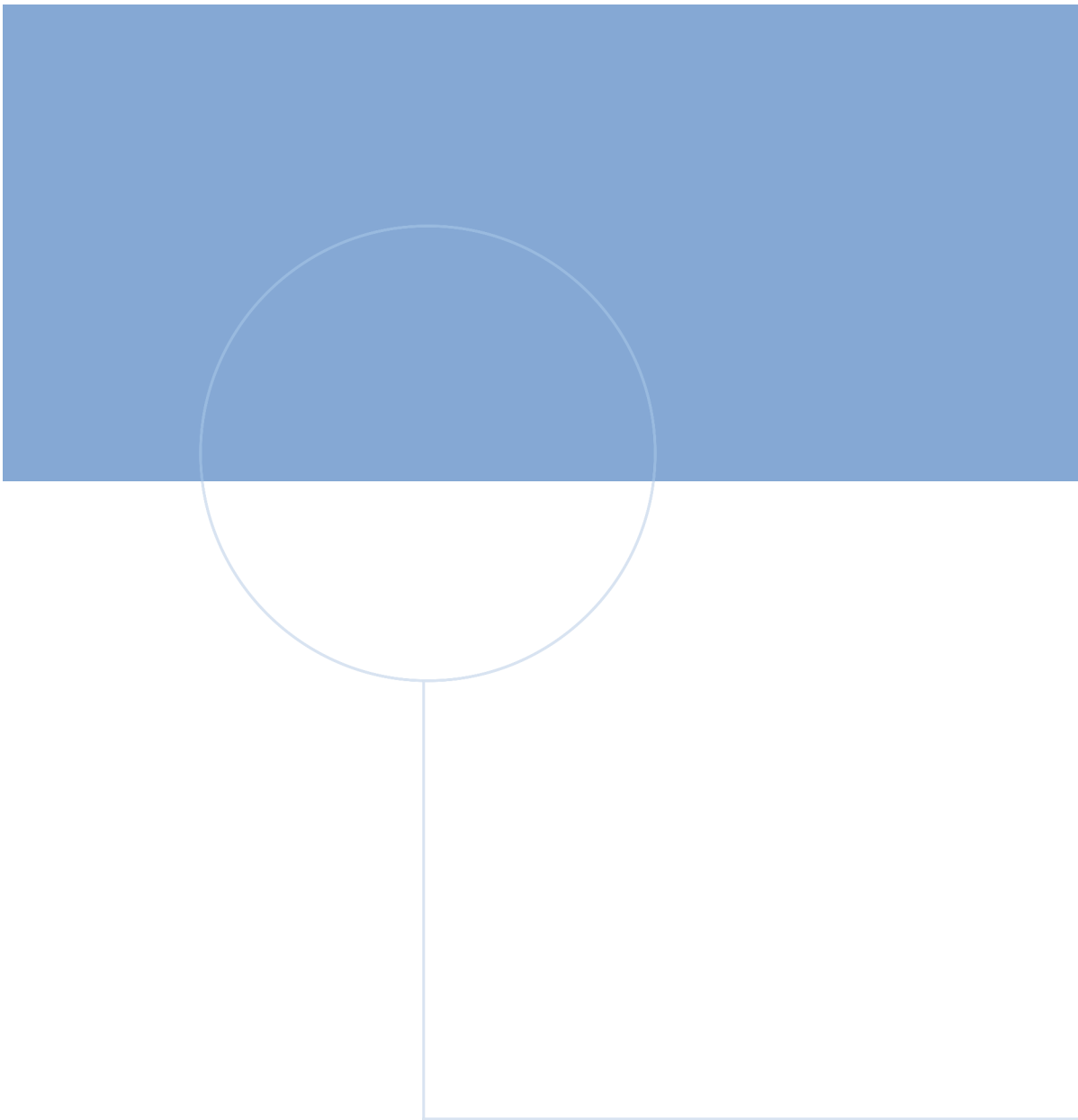

NTNU

Norwegian University of
Science and Technology